An A Priori Analytical Method for the Determination of Operating Reserve Requirements

Aramazd Muzhikyan, *Student Member, IEEE,* Amro M. Farid, *Member, IEEE,* and Kamal Youcef-Toumi, *Member, IEEE*

Abstract

Power balance is one of the key requirements for reliable power system operation. However, factors, such as net load variability and forecast errors, impose practical limitations on matching the scheduled generation and the real–time demand. Normally, potential power imbalances are mitigated by scheduling additional generation capacity called operating reserves. However, reserves are a costly commodity and their requirements should be accurately assessed to avoid unnecessary expense. Currently, the reserve requirements are determined using *a posteriori* methods based upon operator's experience and established assumptions. While these assumptions are made out of a level of engineering practicality, they may not be formally true given the numerical evidence. This paper presents a formal mathematical framework for the *a priori* determination of three types of operating reserve requirements, namely load following, ramping and regulation. Validation of the methodology is performed by a set of extensive simulations that model the power system operations for different scenarios. This methodology is used to study the sensitivity of each type of reserve requirement to the net load and power system parameters.

Index Terms

Power system operations; load following reserves; ramping reserves; regulation reserves.

I. Introduction

POWER balance is one of the key requirements for reliable power system operation. To that end, system operators schedule an appropriate amount of generation to meet the real–time demand. However, factors, such as net load variability and forecast error, impose practical limitations on matching the scheduled generation and the real time demand. Normally, this challenge is overcome by scheduling additional generation capacity called operating reserves. Determination of *appropriate* quantities of these reserves is still an open research question. While power system operation practices, including balancing requirements and classification of reserves, may vary for different regions, the discussions in this paper solely refer to the practices adopted by the U.S. independent system operators (ISO).

The existing industrial practice and academic literature revolves around a similar theme. As discussed in [1], the quantities of reserves are determined *a posteriori* on the basis of historical experience of power system operation. The standard deviation

A. Muzhikyan is with the Department of Engineering Systems and Management, Masdar Institute of Science and Technology, PO Box 54224, Abu Dhabi, UAE. amuzhikyan@masdar.ac.ae

A. M. Farid is with Faculty of Engineering Systems and Management, Masdar Institute of Science and Technology, PO Box 54224, Abu Dhabi, UAE. afarid@masdar.ac.ae

K. Youcef-Toumi is with Faculty of Mechanical Engineering, Massachusetts Institute of Technology, 77 Massachusetts Avenue Cambridge, MA 02139, USA. youcef@mit.edu

Nomenclature

P_L^{peak}	Power system peak load
π	VER penetration level
γ	VER capacity factor
α_L, α_V	Load and VER variabilities
ε_L^{DA}, ε_L^{ST}	Load day-ahead and short-term forecast errors
ρ_L^{DA}, ρ_L^{ST}	Load day-ahead and short-term forecast error autocorrelations
ε_V^{DA}, ε_V^{ST}	VER day-ahead and short-term forecast errors
ρ_V^{DA}, ρ_V^{ST}	VER day-ahead and short-term forecast error autocorrelations
T_s	Data sampling time step
T_h	Day-ahead scheduling (SCUC) time step
T_m	Real-time balancing market (SCED) time step
N_h	Number of samples in T_h interval
N_m	Number of samples in T_m interval
P^{LF}, P^{RP}, P^{RG}	Load following, ramping and regulation reserve requirements
$P(t)$	Actual net load profile
$\hat{P}_{DA}(t)$	Forecasted SCUC schedule
$\hat{P}_{ST}(t)$	Forecasted SCED schedule
$\hat{R}_{DA}(t)$	Forecasted SCUC ramping schedule
$\hat{R}_{ST}(t)$	Forecasted SCED ramping schedule
$\bar{P}_{DA}(t)$, $\bar{P}_{DA}[n]$	Best forecast SCUC schedule
$\bar{P}_{ST}(t)$, $\bar{P}_{ST}[n]$	Best forecast SCED schedule
$\bar{R}_{DA}(t)$, $\bar{R}_{DA}[n]$	Best forecast SCUC ramping schedule
$\bar{R}_{ST}(t)$, $\bar{R}_{ST}[n]$	Best forecast SCED ramping schedule
$\bar{P}_{DA}(\omega)$	Truncated Fourier transform of $\bar{P}_{DA}(t)$, $\bar{P}_{DA}[n]$
$\bar{P}_{ST}(\omega)$	Truncated Fourier transform of $\bar{P}_{ST}(t)$, $\bar{P}_{ST}[n]$
$\bar{R}_{DA}(\omega)$	Truncated Fourier transform of $\bar{R}_{DA}(t)$, $\bar{R}_{DA}[n]$
$\bar{R}_{ST}(\omega)$	Truncated Fourier transform of $\bar{R}_{ST}(t)$, $\bar{R}_{ST}[n]$

of potential imbalances is determined from the net load variability [1], [2], [3] *or* its forecast error [4], [5], [6], [7], [8]. Then, the reserve requirements are defined to cover the appropriate confidence interval in compliance with the North American Electric Reliability Corporation (NERC) balancing requirements [9]. Normally, the load following reserve requirement is chosen $2-3$ times the standard deviation of the imbalances, while the regulation reserve requirement is $5-6$ times [1], [10], [11]. These previous studies make several simplifying assumptions in the modeling that do not necessarily reflect the power system operations knowledge [12], [13], [14]:

Assumption 1. Invariance of the Probability Density Function: The probability density function of imbalances is typically calculated over a long period of analysis (e.g. one year). Its value during the next period will have the same shape as in the current period [1], [10], [11].

Assumption 2. Equivalence of Standard Deviations: The standard deviation of imbalances can equivalently be determined by either the net load variability or its forecast error. Some works use variability [1], [2], [3], while others use the forecast error [4], [5], [6], [7], [8].

Assumption 3. Invariance of the Standard Deviation: The standard deviation of imbalances in the next period of analysis (e.g. a year) will have the same magnitude as in the current period [1].

Assumption 4. Non-dependence on Power System Operator Decisions & Control: The standard deviation of imbalances does not depend on the endogenous parameters of the power system operator decisions and control. According to Assumption 2, it only depends on the variability and forecast error, which can be viewed as exogenous disturbances to the power system operation and control.

While these assumptions have been made out of a level of engineering practicality, they are unlikely to be formally true [15], [16]. Assumption 1 suggests that the power system's stochastic processes retain their characteristics from one year to the next, which has no numerical evidence [17], [18], [19]. A fast adoption of variable energy resources over the course of a year would change this distribution. In regards to Assumption 2, a perfectly forecasted but highly variable net load still requires more load following reserves than a modestly variable net load [15], [16]. Similarly, a high forecast error will require greater reserves than low forecast error [15], [16]. Therefore, the reserve requirement is more likely to depend on both variability and forecast error. Meanwhile, Assumption 3 suggests that the power system does not evolve over the long term (e.g. a year). However, the variables such as variable energy resource (VER) penetration level, forecast error and variability all have the potential to change from year to year. Finally, the recent Federal Energy Regulatory Commission (FERC) requirement [20] to change the minimum frequency of the balancing market from one hour to 15 minutes suggests that power system imbalances do depend on the power system's endogenous characteristics contrary to Assumption 4.

Recently, operating reserve requirement assessment *dynamic* methods have been discussed in the literature [21], [22], [23], [24], [25]. The traditional *static* methods, currently used in the industry, assess the reserve requirements for the whole observed time period (e.g. one year). In contrast, the dynamic methods take advantage of the fact that the operating reserve requirements vary as the VER generation forecast and the grid conditions change. As a result, the operating reserve requirements assessed by dynamic methods vary for different time periods (e.g. hourly), which is likely to produce significant cost savings. While the rationale of these methods is empirically strong, they still follow Assumptions 1–4. This work proceeds explicitly avoiding these assumptions.

An *a priori* analytical framework for the determination of different types of operating reserve requirements is introduced in [12], [13], [14], where each reserve requirement is presented as an analytical function of the *principal parameters*, namely VER penetration level, VER capacity factor, load and VER variabilities, load and VER forecast errors, scheduling and balancing time steps. While the goal of [12], [13], [14] is to propose a reserve requirement calculation analytical framework, this paper demonstrates the proposed methodology to study the sensitivity of each type of reserve requirements to the net load and power system parameters. This is an essential part of describing how the VER integration affects the operating reserve requirements in normal operation and helps to better accommodate the VER in power systems. This paper extends the findings of [12], [13], [14] with the following three contributions. First, the dependence of the load following and ramping reserve requirements on the balancing time step is neglected in [12], [13], [14]. This assumption is true for small time steps discussed in [12], [13], [14] ($\sim 5min$). However, for relatively larger balancing time steps this assumption may no longer hold. To that end, this paper generalizes the load following and ramping reserve requirement calculation methodology with the incorporation of the balancing time step. Second, a comprehensive numerical validation of the proposed methodology is conducted. Both the accuracy of the calculations and the balancing performance of the system for the calculated reserve amounts are tested for a wide range of scenarios. Finally, the sensitivity of the operating reserve requirements to the principal parameters is studied.

The derivations of these analytical functions follow a simple approach. Since the goal of the operating reserves is to mitigate power system imbalances, the reserve requirements should be directly defined by the magnitudes of these imbalances. For that reason, this paper starts the determination of the reserve requirements by studying the imbalances that occur at different time scales of power system operations. Here, the imbalances are modeled as time series with explicitly incorporated VER and power system operations parameters. This allows generating imbalances for different VER integration and power system

operation potential scenarios by varying these parameters. Next, a family of probability distributions of imbalance time series are generated by varying the mentioned parameters for wide ranges of different values. The study of these probability distributions proves the hypothesis that the reserve requirements are *proportional* to the standard deviations of the corresponding imbalances. The probability distributions also allow calculating the multiplier of the standard deviation that covers 90% of the imbalances to meet the NERC balancing standard. As the final step, the standard deviations of the imbalances are derived as analytical functions of the mentioned parameters using the imbalance models mentioned above.

This paper is organized as follows: Section II provides the background information, Section III briefly describes the methodology, Section IV validates the analytical calculations by a set of simulations, Section V studies the sensitivity of each type of reserve requirement to the principal parameters and Section VI draws the conclusions.

II. Background

This section presents the background material necessary for the development and validation of the operating reserve requirement calculation methodology, and consists of three subsections. The first subsection introduces the fundamental definitions of the concepts used in the paper. Next, the power system enterprise control simulator is briefly described, which is used to test the performance of the power system balancing operations when the reserve requirements are calculated according to the presented methodology. The third subsection discusses the choice of the power system balancing performance criterion.

A. Fundamental definitions

The definitions presented in this subsection can be divided into three groups. The first group defines the three types of reserves considered in this paper, namely load following, ramping and regulation. The second group of definitions is related to the VER and load statistical parameters, such as variabilities and forecast errors. The third group introduces a set of auxiliary profiles that are used in the calculations of the operating reserve requirements.

This paper considers three types of operating reserves, namely load following, ramping and regulation, as defined below.

Definition 1. *Load following reserve:* Capacity available during normal operations for assistance in active power balance to correct the future anticipated imbalance (upward and downward). Activated by the real-time market (SCED) [26], [27].

Definition 2. *Ramping reserve:* Capacity available for assistance in active power balance during infrequent events that are more severe than balancing needed during normal conditions and is used to correct non-instantaneous imbalances (upward and downward). Activated by the real-time market (SCED) [26], [27].

Definition 3. *Regulation reserve:* Capacity available during normal operations for assistance in active power balance to correct the current imbalance (upward and downward). Activated by the regulation service (AGC) [26], [27].

Next, the second group of definitions is related to the VER and load statistical parameters.

Definition 4. *VER Penetration Level:* The installed VER capacity P_V^{max} normalized by the system peak load P_L^{peak} [28]:

$$\pi = \frac{P_V^{max}}{P_L^{peak}} \tag{1}$$

Definition 5. *VER Capacity Factor:* The average VER output $P_V(t)$ per installed capacity taken over a period T (e.g. one year) [12], [13], [14]:

$$\gamma = \frac{\overline{P_V(t)}}{P_V^{max}} \tag{2}$$

Definition 6. *Variability:* The variability of $P(t)$ profile is the root-mean-square of that profile's rate of change normalized by the root-mean-square of that profile [12], [13], [14]:

$$A = \frac{rms\left(\frac{\mathrm{d}P(t)}{\mathrm{dt}}\right)}{rms\Big(P(t)\Big)} \tag{3}$$

One way of manipulating the variability of the profile is temporal scaling. Assume that the profile $P_0(t)$ has a variability A_0 and $P(t)$ is defined as:

$$P(t) = P_0(\alpha t) \tag{4}$$

According to (3):

$$A = \frac{rms\left(\frac{\mathrm{d}P(t)}{\mathrm{dt}}\right)}{rms\Big(P(t)\Big)} = \frac{rms\left(\frac{\mathrm{d}P_0(\alpha t)}{\mathrm{dt}}\right)}{rms\Big(P_0(\alpha t)\Big)} = \alpha \cdot \frac{rms\left(\frac{\mathrm{d}P_0(\alpha t)}{\mathrm{d}(\alpha \mathrm{t})}\right)}{rms\Big(P_0(\alpha t)\Big)} = \alpha \cdot \frac{rms\left(\frac{\mathrm{d}P_0(t)}{\mathrm{dt}}\right)}{rms\Big(P_0(t)\Big)} = \alpha A_0 \tag{5}$$

Thus, α can be considered as the normalized variability of $P(t)$ profile:

$$\alpha = \frac{A}{A_0} \tag{6}$$

Next in this group are definitions regarding forecast errors. The forecast error indicates the deviation between the actual and forecasted values and can be defined by various measures such as mean absolute error (MAE), mean square error (MSE) [29]. This paper uses the latter which suits the operating reserve requirement calculation methodology better. Both day–ahead and short–term forecast errors are defined identically, hence, *DA* and *ST* superscripts are omitted. The load and VER forecast errors are normalized by the peak load and the installed capacity respectively.

Definition 7. *Best Day–Ahead Forecast*: The best day–ahead forecast of $P(t)$ profile is equivalent to the average value of that profile during the k^{th} day–ahead scheduling time block of duration T_h [12]:

$$\bar{P}^{DA}[k] = \frac{1}{T_h} \int_{kT_h}^{(k+1)T_h} P(t)\mathrm{dt} \tag{7}$$

Definition 8. *Best Short–Term Forecast*: The best short–term forecast of $P(t)$ profile is equivalent to its actual value at kT_m [14]:

$$\bar{P}^{ST}[k] = P(kT_m) \tag{8}$$

Definition 9. *Load Forecast Error:* The standard deviation of the difference between the best and the actual load forecasts normalized by the peak load [12], [13], [14]:

$$\varepsilon_L = \frac{\sqrt{\frac{1}{n}\sum_{k=0}^{n}\left(\bar{P}_L[k] - \hat{P}_L[k]\right)^2}}{P_L^{peak}} \tag{9}$$

Definition 10. *VER Forecast Error:* The standard deviation of the difference between the best and the actual VER forecasts normalized by the installed VER capacity [12], [13], [14]:

$$\varepsilon_V = \frac{\sqrt{\frac{1}{n}\sum_{k=0}^{n}\left(\bar{P}_V[k] - \hat{P}_V[k]\right)^2}}{P_V^{max}} \tag{10}$$

Definition 11. *Forecast Error Autocorrelation:* The single-step autocorrelation of the difference between the best and the actual forecasts:

$$\rho = \sqrt{\frac{\sum_{k=0}^{n-1}\left(\bar{P}[k+1] - \hat{P}[k+1]\right)\left(\bar{P}[k] - \hat{P}[k]\right)}{\sum_{k=0}^{n}\left(\bar{P}[k] - \hat{P}[k]\right)^2}} \tag{11}$$

This work assumes that both load and VER forecast errors have zero average [30]:

$$\sum_{k=0}^{n}\left(\bar{P}[k] - \hat{P}[k]\right) = \sum_{k=0}^{n}\left(\bar{P}_L[k] - \hat{P}_L[k]\right) = \sum_{k=0}^{n}\left(\bar{P}_V[k] - \hat{P}_V[k]\right) = 0 \tag{12}$$

It also assumes that any shifted copies of VER and load forecast errors are uncorrelated [30], i.e., for any integer m:

$$\sum_{k=0}^{n}\left(\bar{P}_L[k] - \hat{P}_L[k]\right)\left(\bar{P}_V[k+m] - \hat{P}_V[k+m]\right) = 0 \tag{13}$$

Finally, the third group of definitions introduces a set of auxiliary profiles that are used in the calculations of the operating reserve requirements and are depicted in Fig. 1. These definitions are applicable to either of load, VER and net load profiles.

Definition 12. *Best Day–Ahead Forecast Profile*: A stepwise constant time series with the value of the best day–ahead forecast over the corresponding T_h interval [12]:

$$\bar{P}^{DA}(t) = \bar{P}^{DA}[k], \qquad kT_h < t \leq (k+1)T_h \tag{14}$$

Definition 13. *Actual Day-Ahead Forecast Profile*: A stepwise constant time series with the value of the actual day–ahead forecast over the corresponding T_h interval [12]:

$$\hat{P}^{DA}(t) = \hat{P}^{DA}[k], \qquad kT_h < t \leq (k+1)T_h \tag{15}$$

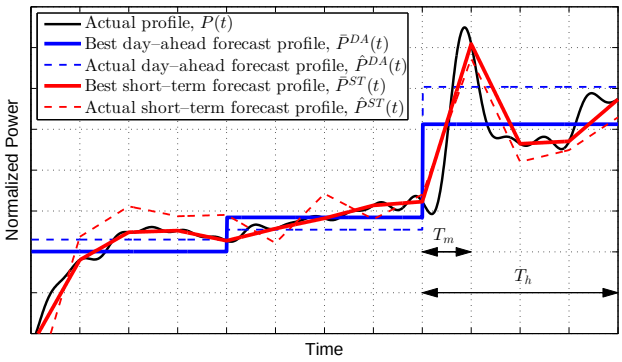

Fig. 1: The comparison of actual, best day-ahead forecast, actual day-ahead forecast, best short-term forecast and actual short-term forecast profiles

Definition 14. *Best Short-Term Forecast Profile*: A piecewise linear function that connects the samples with T_m interval [14]:

$$\bar{P}^{ST}(t) = \bar{P}^{ST}[k] + \frac{\bar{P}^{ST}[k+1] - \bar{P}^{ST}[k]}{T_m} \cdot (t - kT_m), \qquad kT_m < t \leq (k+1)T_m \tag{16}$$

Definition 15. *Actual Short-Term Forecast Profile*: A piecewise linear function that connects the short-term forecast samples with T_m interval [14]:

$$\hat{P}^{ST}(t) = \hat{P}^{ST}[k] + \frac{\hat{P}^{ST}[k+1] - \hat{P}^{ST}[k]}{T_m} \cdot (t - kT_m), \qquad kT_m < t \leq (k+1)T_m \tag{17}$$

Definition 16. *Best Day-Ahead Ramping Forecast Profile*: A stepwise constant time series with the value of the best day-ahead ramping forecast over the corresponding T_h interval [13]:

$$\bar{R}^{DA}(t) = \frac{\bar{P}^{DA}[k+1] - \bar{P}^{DA}[k]}{T_h}, \qquad kT_h < t \leq (k+1)T_h \tag{18}$$

Definition 17. *Actual Day-Ahead Ramping Forecast Profile*: A stepwise constant time series with the value of the day-ahead ramping forecast over the corresponding T_h interval [13]:

$$\hat{R}^{DA}(t) = \frac{\hat{P}^{DA}[k+1] - \hat{P}^{DA}[k]}{T_h}, \qquad kT_h < t \leq (k+1)T_h \tag{19}$$

Definition 18. *Best Short-Term Ramping Forecast Profile*: A stepwise constant time series with the value of the best short-term ramping forecast over the corresponding T_m interval [13]:

$$\bar{R}^{ST}(t) = \frac{\bar{P}^{ST}[k+1] - \bar{P}^{ST}[k]}{T_m}, \qquad kT_m < t \leq (k+1)T_m \tag{20}$$

B. Power system enterprise control

Power system operations can be modeled as a multi–layer control hierarchy on top of the physical power grid as shown in Fig. 2. The control layers considered in this study are resource scheduling, balancing actions and the regulation service as consistent with [31], [32]. Each consecutive control operates at a smaller timescale, that allows successive imbalance mitigation.

The resource scheduling is performed by the security–constrained unit commitment (SCUC) [33] that uses the day–ahead net load forecast to schedule generation that meets the real–time demand. Since the day–ahead forecast is not perfect and the SCUC has a limited time resolution T_h, the scheduled generation and ramping capabilities do not match the real–time requirements, and imbalances remain at the SCUC output. The mismatch term is the difference between the ideal real–time dispatching schedule (best short–term forecast profile) and the SCUC scheduled generation based on the day-ahead forecast (actual day–ahead forecast profile):

$$\Delta P^{DA}(t) = \bar{P}^{ST}(t) - \hat{P}^{DA}(t) \tag{21}$$

Similarly, the mismatch term for the scheduled ramping resources can be written as:

$$\Delta R^{DA}(t) = \bar{R}^{ST}(t) - \hat{R}^{DA}(t) \tag{22}$$

The balancing actions layer combines the security–constrained economic dispatch (SCED) and manual operator actions. This work restricts its scope to normal operations and, hence, considers only the SCED in the balancing layer. The SCED re–dispatches the generation based on the short–term net load forecast. Since the short–term forecast is not perfect and the

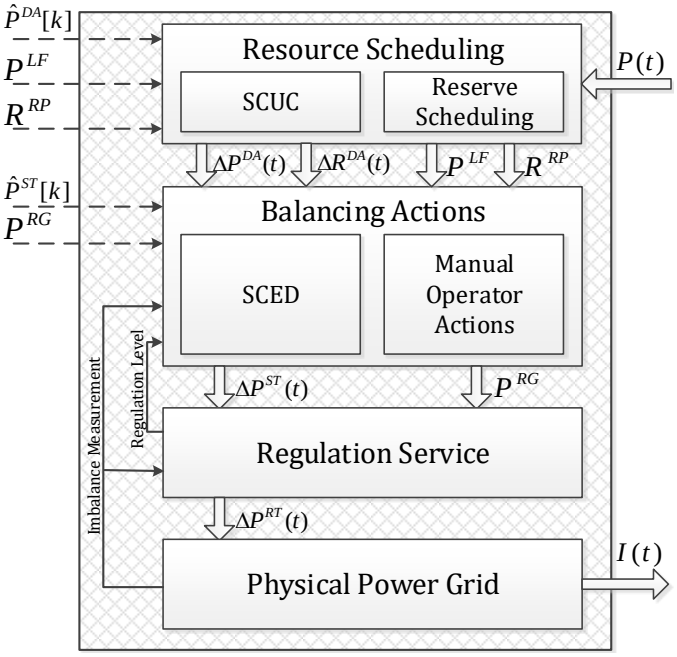

Fig. 2: A multi-layer power grid enterprise control model [31], [32]

SCED has a limited time resolution T_m, the dispatched generation does not match the actual net load, and imbalances remain at the SCED output. The mismatch term at this stage is the difference between the actual net load and the SCED dispatched generation based on the short-term forecast (best short–term forecast profile):

$$\Delta P^{ST}(t) = P(t) - \hat{P}^{ST}(t) \tag{23}$$

The regulation service layer is implemented as an automatic generation control (AGC). The AGC responds to the current imbalance level and moves the generation to the opposite direction until either the imbalance is mitigated or the available regulation reserve is fully used. The imbalance at the output of the regulation service layer is further mitigated by the load response and system inertia.

Power system operators procure additional generation resources called operating reserves to mitigate mismatches (21)– (23) at different stages of occupance. This paper uses the classification of reserves found in [26], [27], recognizing that there is no universal agreement upon operating reserves classification scheme. The interested reader is referred to other classification schemes in academia and industry across several geographies [34], [35]. Three types of reserves are studied, namely load following, ramping and regulation. These reserves are used as a part of normal operations rather than after a contingency. Ultimately, the chosen classification scheme 1.) is consistent with operations in several American ISO's and 2.) lends itself to validation by recent work on power system enterprise control [31], [32], [36]. In American operations, load following and regulation reserves are offered as monetized market products while ramping is not. Operating reserve requirements can also be fulfilled by energy storage [37], [36] and demand side management resources [38].

C. Balancing performance criterion

The balancing performance of American ISO's is regulated by North American Electric Reliability Corporation (NERC) *Standard BAL–001–0.1a* [9]. Four requirements constituting this standard define the permissable levels of the Area Control Error (ACE) or the imbalance. In particular, the second requirement or the Control Performance Standard 2 (CPS2) states that each balancing authority shall operate such that its average ACE for at least 90% of clock–ten–minute periods (6 non–overlapping periods per hour) during a calendar month is within a specific limit called the L_{10}. As of August 2006, PJM is participating in the NERC field test which has established a new balancing metric, Balancing Authority ACE Limit (BAAL), as a possible substitute for CPS2 [39]. According the new standard, each Balancing Authority shall operate such that its clock–minute average of Reporting ACE does not exceed its clock–minute BAAL for more than 30 consecutive clock-minutes, for the applicable Interconnection in which the Balancing Authority operates [40]. This paper limits its discussion to only one area with no net import/export.

While the CPS is a well–established criterion for power system balance diagnosis, its use for this study is limited for the following reasons. Being a function of the ACE, the CPS only defines the percentage of intervals with a residual imbalance, while the actual magnitude of the imbalance is ignored. This may bring about misleading results about the impact of the reserve requirements on the imbalances. With increase of the reserve requirements the magnitude of the imbalance (the standard

deviation) reduces monotonically. However, as shown in [31], [32], the curves for CPS are not monotonic and at some points the value of CPS even decreases with increase of reserve requirements. These results are hard to interpret. Also, the CPS value depends on system–specific L_{10} threshold whose value varies for different systems. This further complicates the interpretation of the CPS value. To avoid these issues, the standard deviation of imbalances is used as a balancing performance criterion in this study.

III. Operating Reserve Requirement Calculation Methodology

While the reserve requirement determination techniques available in the literature are driven by Assumptions 1–4, this paper invalidates these assumptions and instead demonstrates an analytical framework to determine the load following, ramping and regulation reserve requirements as explicit analytical expressions of the principal parameters:

$$P^{LF}\left(\pi,\gamma,\alpha_L,\alpha_V,\varepsilon_L^{DA},\varepsilon_V^{DA},T_h,T_m\right) \tag{24}$$

$$R^{RP}\left(\pi,\gamma,\alpha_L,\alpha_V,\varepsilon_L^{DA},\varepsilon_V^{DA},T_h,T_m\right) \tag{25}$$

$$P^{RG}\left(\pi,\gamma,\alpha_L,\alpha_V,\varepsilon_L^{ST},\varepsilon_V^{ST},T_m\right) \tag{26}$$

These expressions allow an *a priori* determination of how the operating reserve requirements evolve with power system changes and, therefore, are sufficient to comprehensively test the validity of Assumptions 1–4. It is important to notice that due to the difference in the operating time scales, the load following and ramping reserve requirements depend on the load and VER day–ahead forecast errors, while the regulation reserve requirement depends on the short–term forecast errors. Also, since the regulation operates at smaller time scale it is not dependent on the much larger scheduling time step.

This section briefly describes the methodology for calculation of the reserve requirements in the form of (24)–(26). The reader is advised to refer to [12], [13], [14] for the detailed derivations.

A. The strategy

Procurement of load following, ramping and regulation reserves intends to mitigate the imbalance terms (21)–(23) respectively. Therefore, the reserve requirements are expected to depend on the magnitudes of the corresponding imbalance terms. To that end, the following hypothesis, relating the reserve requirements and the standard deviations of the corresponding mismatch terms, is proposed.

Hypothesis. The load following, ramping and regulation reserve requirements are proportional to the standard deviations of the imbalance terms (21)–(23) respectively:

$$P^{LF} = \beta^{LF}\sigma^{LF} \tag{27}$$

$$R^{RP} = \beta^{RP}\sigma^{RP} \tag{28}$$

$$P^{RG} = \beta^{RG}\sigma^{RG} \tag{29}$$

where β^{LF}, β^{RP} and β^{RG} multipliers are independent of the principal parameters.

This hypothesis is tested by studying the probability distributions of the mismatch terms (21)–(23) under a variety of scenarios, which also helps to test the validity of Assumption 1. To that end, families of probability distributions are generated for each imbalance term by varying the principal parameters and comparing the values of β^{LF}, β^{RP}, β^{RG} multipliers.

Next, analytical expressions for the standard deviations of mismatch terms (21)–(23) are derived as explicit functions of the principal parameters:

$$\sigma^{LF}\left(\pi,\gamma,\alpha_L,\alpha_V,\varepsilon_L^{DA},\varepsilon_V^{DA},T_h,T_m\right) \tag{30}$$

$$\sigma^{RP}\left(\pi,\gamma,\alpha_L,\alpha_V,\varepsilon_L^{DA},\varepsilon_V^{DA},T_h,T_m\right) \tag{31}$$

$$\sigma^{RG}\left(\pi,\gamma,\alpha_L,\alpha_V,\varepsilon_L^{ST},\varepsilon_V^{ST},T_m\right) \tag{32}$$

This strategy gains further importance by virtue of the fact that the major part of the derivations is carried out in the frequency domain. While the time and frequency domain representations carry identical information, the frequency domain representation allows better interpretation of the final analytical expressions (24)–(26). In particular, the derivations are carried out using the auxiliary profiles introduced in Definitions 12–18 that depend on temporal parameters, such as day–ahead scheduling (T_h) and real-time balancing (T_m) time steps. However, the way temporal parameters appear in (14)–(20) leaves little room for interpretation of their impact on reserve requirements. In contrast, frequency domain representation enables explicit incorporation of temporal parameters into reserve requirements equations. Also, the previous work in the literature has shown that while VER and load time profiles vary widely for different cases, their power spectra remain invariant [41], [42]. Therefore, the frequency domain representation allows better accommodation of the historical data into the derivations.

B. The mismatch terms

To study the probability distributions of the mismatch terms (21)–(23) for different scenarios, the principal parameters need to be explicitly integrated into their expressions. Using (1), (2), (4), the load and VER profiles can be modeled as:

$$P_L(t) = \frac{P_L(t)}{P_L^{peak}} \cdot P_L^{peak} = p_L(t) \cdot P_L^{peak} = p_L^0(\alpha_L t) \cdot P_L^{peak} \tag{33}$$

$$P_V(t) = \frac{P_V(t)}{\overline{P_V(t)}} \cdot \frac{\overline{P_V(t)}}{P_V^{max}} \cdot \frac{P_V^{max}}{P_L^{peak}} \cdot P_L^{peak} = p_V(t) \cdot \gamma \cdot \pi \cdot P_L^{peak} = p_V^0(\alpha_V t) \cdot \gamma \cdot \pi \cdot P_L^{peak} \tag{34}$$

where $p_L^0(t)$ and $p_V^0(t)$ are load and VER profiles normalized by the peak load and the average VER output respectively. Using (33) and (34), the load and VER ramping profiles can be modeled as:

$$R_L(t) = \frac{\mathrm{d}P_L(t)}{\mathrm{dt}} = \frac{\mathrm{d}\left(p_L^0(\alpha_L t) P_L^{peak}\right)}{\mathrm{dt}} = \frac{\mathrm{d}\left(p_L^0(\alpha_L t)\right)}{\mathrm{d}\left(\alpha_L t\right)} \cdot \alpha_L \cdot P_L^{peak} = r_L^0(\alpha_L t) \cdot \alpha_L \cdot P_L^{peak} \tag{35}$$

$$R_V(t) = \frac{\mathrm{d}P_V(t)}{\mathrm{dt}} = \frac{\mathrm{d}\left(p_V^0(\alpha_V t) \cdot \gamma \cdot \pi \cdot P_L^{peak}\right)}{\mathrm{dt}} = \frac{\mathrm{d}\left(p_V^0(\alpha_V t)\right)}{\mathrm{d}\left(\alpha_V t\right)} \cdot \alpha_V \cdot \gamma \cdot \pi \cdot P_L^{peak} = r_V^0(\alpha_V t) \cdot \alpha_V \cdot \gamma \cdot \pi \cdot P_L^{peak} \tag{36}$$

where $r_L^0(t)$ and $r_V^0(t)$ are time derivatives of $p_L^0(t)$ and $p_V^0(t)$ respectively. According to (35)–(36), the load and VER ramping rates are proportional to their corresponding variabilities, which adds credibility to the definition of variability (3). Load and VER models (33)–(36) are now used to explicitly incorporate the principal parameters into the mismatch terms (21)–(23) as follows:

$$\Delta P^{DA}(t) = \left(\left(\bar{p}_L^{ST}(\alpha_L t) - \bar{p}_L^{DA}(\alpha_L t) \right) - \gamma \cdot \pi \cdot \left(\bar{p}_V^{ST}(\alpha_V t) - \bar{p}_V^{DA}(\alpha_V t) \right) + \varepsilon_L^{DA} \cdot \xi_L^{DA}(t) - \varepsilon_V^{DA} \cdot \pi \cdot \xi_V^{DA}(t) \right) \cdot P_L^{peak} \tag{37}$$

$$\begin{aligned} \Delta R^{DA}(t) = \Bigg(& \alpha_L \cdot \left(\bar{r}_L^{ST}(\alpha_L t) - \bar{r}_L^{DA}(\alpha_L t) \right) - \alpha_V \cdot \gamma \cdot \pi \cdot \left(\bar{r}_V^{ST}(\alpha_V t) - \bar{r}_V^{DA}(\alpha_V t) \right) + \\ & + \varepsilon_L^{DA} \cdot \frac{\sqrt{2\left(1 - \left(\rho_L^{DA}\right)^2\right)}}{T_h} \cdot \zeta_L^{DA}(t) - \varepsilon_V^{DA} \cdot \frac{\sqrt{2\left(1 - \left(\rho_V^{DA}\right)^2\right)}}{T_h} \cdot \pi \cdot \zeta_V^{DA}(t) \Bigg) \cdot P_L^{peak} \end{aligned} \tag{38}$$

$$\begin{aligned} \Delta P^{ST}(t) = \Bigg(& \left(p_L(\alpha_L t) - \bar{p}_L^{ST}(\alpha_L t) \right) - \gamma \cdot \pi \cdot \left(p_V(\alpha_V t) - \bar{p}_V^{ST}(\alpha_V t) \right) + \\ & + \varepsilon_L^{ST} \cdot \sqrt{\frac{2 + \left(\rho_L^{ST}\right)^2}{3}} \cdot \xi_L^{ST}(t) - \varepsilon_V^{ST} \cdot \sqrt{\frac{2 + \left(\rho_V^{ST}\right)^2}{3}} \cdot \pi \cdot \xi_V^{ST}(t) \Bigg) \cdot P_L^{peak} \end{aligned} \tag{39}$$

where $\xi_L(t)$ and $\xi_V(t)$ denote load and VER forecast error time series respectively, normalized to unit standard deviations. Similarly, $\zeta_L^{DA}(t)$ and $\zeta_V^{DA}(t)$ are load and VER ramping forecast error time series respectively, normalized to unit standard deviations. The derivations of (37)–(39) can be found in Appendix.

C. Probability distributions of the mismatch terms

To verify the hypothesis proposed in Section III-A, the probability distributions of the mismatch terms (21)–(23) are studied under a variety of scenarios, which also helps to test the validity of Assumption 1. To that end, a family of probability distributions is generated for each imbalance term by varying the principal parameters in (37)–(39) for a wide range of values. Fig. 3–5 show the associated families of probability distributions of the mismatch terms (21)–(23) respectively, normalized to unit standard deviations. The load and wind data are taken from the Bonneville Power Administration (BPA) repositories [43]. Here, the probability distributions largely differ from each other within each family, which contradicts Assumption 1. However, from the perspective of sizing the reserve requirements, the cumulative percentage of the mismatch captured by the given interval is more relevant. To that end, the associated family of cumulative distribution functions (CDF) are also represented on the corresponding plots. Although there is still a significant difference amongst curves within each family, in the scope of this work only the interval that capture 90% of the mismatch is of the most interest to comply with the NERC balancing requirements mentioned above. The 90% intervals generally agree within each family for the wide ranges of principal parameters, as shown in Table I. Here, the minimum, maximum values and the variation of β^{LF}, β^{RP}, β^{RG} multipliers are presented, where variation is the standard deviation of the given multiplier's value for different scenarios normalized by its

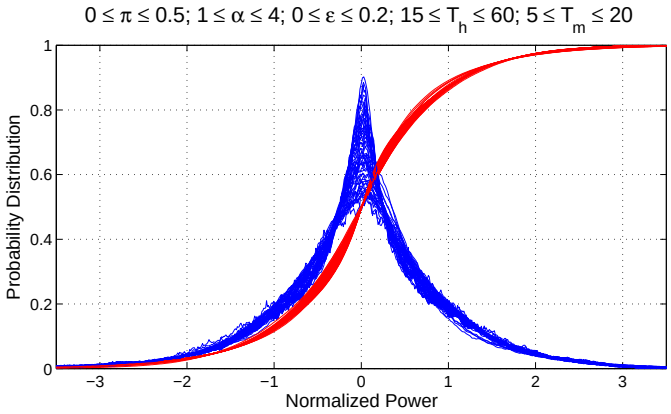

Fig. 3: Probability density and cumulative density functions of the mismatch term $\Delta P^{DA}(t)$ for different values of principal parameters

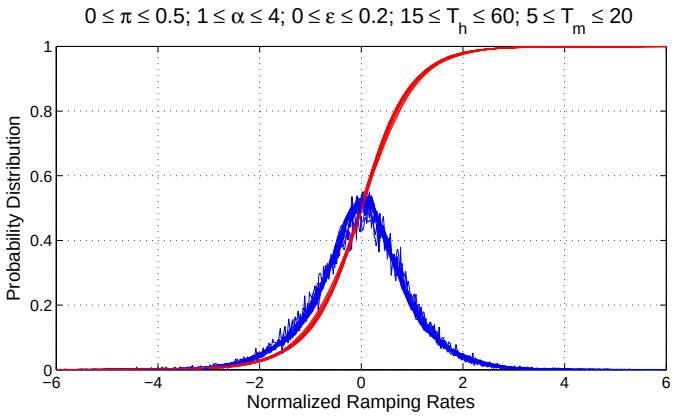

Fig. 4: Probability density and cumulative density functions of the mismatch term $\Delta R^{DA}(t)$ for different values of principal parameters

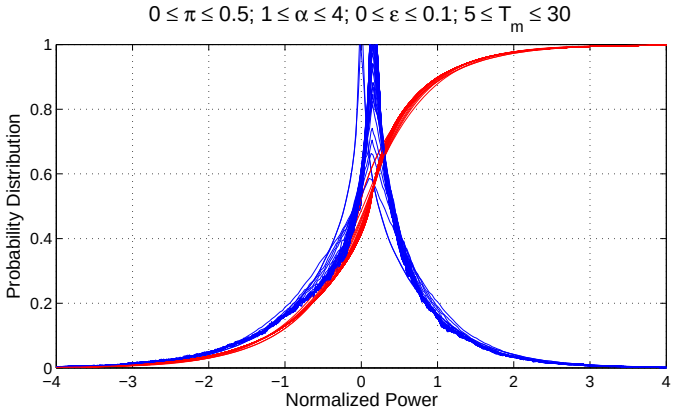

Fig. 5: Probability density and cumulative density functions of the mismatch term $\Delta P^{ST}(t)$ for different values of principal parameters

TABLE I: The variations of β^{LF}, β^{RP}, β^{RG} multipliers for different scenarios

Percentage	β^{LF}			β^{RP}			β^{RG}		
	min	max	variation	min	max	variation	min	max	variation
5%	−1.6638	−1.6221	0.0053	−1.6812	−1.5692	0.0156	−1.7671	−1.6373	0.0146
95%	1.5858	1.6447	0.0054	1.5070	1.5962	0.0129	1.4727	1.5632	0.0124

mean. Since the variation for any scenario is less than 2% of the mean, the proposed hypothesis can be considered true. The maximum values of each multiplier are chosen for reserve requirement calculations to make sure the captured confidence interval is at least 90% for any scenario:

$$\beta^{LF} \approx 1.66 \tag{40}$$
$$\beta^{RP} \approx 1.68 \tag{41}$$
$$\beta^{RG} \approx 1.77 \tag{42}$$

D. Standard deviations of the mismatch terms

Once the hypothesis in Section III-A is validated and the values of β^{LF}, β^{RP} and β^{RG} are obtained, this paper proceeds to derivations of the standard deviations of the mismatch terms in accordance to (30)–(32). The models of the mismatch terms (37)–(39) with incorporated parameters are used for the derivations. It can be shown that ΔP_α and ΔP_ε components in (37)–(39) are statistically independent for each mismatch term [12], [13], [14], and, therefore, the standard deviation of each mismatch term can be split into two components related to the net load variability and forecast error [12], [13], [14]:

$$\left(\sigma^{LF}\right)^2 = \left(\sigma_\varepsilon^{LF}\right)^2 + \left(\sigma_\alpha^{LF}\right)^2 \tag{43}$$
$$\left(\sigma^{RP}\right)^2 = \left(\sigma_\varepsilon^{RP}\right)^2 + \left(\sigma_\alpha^{RP}\right)^2 \tag{44}$$
$$\left(\sigma^{RG}\right)^2 = \left(\sigma_\varepsilon^{RG}\right)^2 + \left(\sigma_\alpha^{RG}\right)^2 \tag{45}$$

where σ_α terms are defined by the load and VER variabilities and can be derived from (37)–(39) respectively as equal to [12], [13], [14]:

$$\left(\sigma_\alpha^{LF}\right)^2 = \left(\left(\sigma_\alpha^{LF}\right)_{LL}^2 + (\gamma\pi)^2 \cdot \left(\sigma_\alpha^{LF}\right)_{VV}^2 - 2\gamma\pi \cdot \left(\sigma_\alpha^{LF}\right)_{LV}^2\right) \cdot \left(P_L^{peak}\right)^2 \tag{46}$$
$$\left(\sigma_\alpha^{RP}\right)^2 = \left(\alpha_L^2 \cdot \left(\sigma_\alpha^{RP}\right)_{LL}^2 + (\alpha_V\gamma\pi)^2 \cdot \left(\sigma_\alpha^{RP}\right)_{VV}^2 - 2\alpha_L\alpha_V\gamma\pi \cdot \left(\sigma_\alpha^{RP}\right)_{LV}^2\right) \cdot \left(P_L^{peak}\right)^2 \tag{47}$$
$$\left(\sigma_\alpha^{RG}\right)^2 = \left(\left(\sigma_\alpha^{RG}\right)_{LL}^2 + (\gamma\pi)^2 \cdot \left(\sigma_\alpha^{RG}\right)_{VV}^2 - 2\gamma\pi \cdot \left(\sigma_\alpha^{RG}\right)_{LV}^2\right) \cdot \left(P_L^{peak}\right)^2 \tag{48}$$

Similarly, σ_ε terms are defined by the load and VER forecast errors and can be derived from (37)–(39) respectively as equal to [12], [13], [14]:

$$\left(\sigma_\varepsilon^{LF}\right)^2 = \left(\left(\varepsilon_L^{DA}\right)^2 + \left(\varepsilon_V^{DA}\right)^2 \cdot \pi^2\right) \cdot \left(P_L^{peak}\right)^2 \tag{49}$$
$$\left(\sigma_\varepsilon^{RP}\right)^2 = \left(\left(\varepsilon_L^{DA}\right)^2 \cdot \frac{2\left(1-\left(\rho_L^{DA}\right)^2\right)}{T_h^2} + \left(\varepsilon_V^{DA}\right)^2 \cdot \frac{2\left(1-\left(\rho_V^{DA}\right)^2\right)}{T_h^2} \cdot \pi^2\right) \cdot \left(P_L^{peak}\right)^2 \tag{50}$$
$$\left(\sigma_\varepsilon^{RG}\right)^2 = \left(\left(\varepsilon_L^{ST}\right)^2 \cdot \frac{2+\left(\rho_L^{ST}\right)^2}{3} + \left(\varepsilon_V^{ST}\right)^2 \cdot \frac{2+\left(\rho_V^{ST}\right)^2}{3} \cdot \pi^2\right) \cdot \left(P_L^{peak}\right)^2 \tag{51}$$

The terms $\left(\sigma_\alpha^{LF}\right)_{XY}$, $\left(\sigma_\alpha^{RP}\right)_{XY}$ and $\left(\sigma_\alpha^{RG}\right)_{XY}$ in (46)–(48) are the standard deviations of the differences between the normalized profiles found in (37)–(39) respectively, where the 'XY' subscript denotes either of 'LL', 'VV', 'LV'. As mentioned above, the derivations of these terms are converted into the frequency domain using Parseval's theorem [12], [13], [14]:

$$\left(\sigma_\alpha^{LF}\right)_{XY}^2 = \int_{-\infty}^{+\infty} E\left[\left(\bar{P}_X^{ST}(\omega) - \bar{P}_X^{DA}(\omega)\right)^* \cdot \left(\bar{P}_Y^{ST}(\omega) - \bar{P}_Y^{DA}(\omega)\right)\right] \mathrm{d}\omega \tag{52}$$
$$\left(\sigma_\alpha^{RP}\right)_{XY}^2 = \int_{-\infty}^{+\infty} E\left[\left(\bar{R}_X^{ST}(\omega) - \bar{R}_X^{DA}(\omega)\right)^* \cdot \left(\bar{R}_Y^{ST}(\omega) - \bar{R}_Y^{DA}(\omega)\right)\right] \mathrm{d}\omega \tag{53}$$
$$\left(\sigma_\alpha^{RG}\right)_{XY}^2 = \int_{-\infty}^{+\infty} E\left[\left(P_X(\omega) - \bar{P}_X^{ST}(\omega)\right)^* \cdot \left(P_Y(\omega) - \bar{P}_Y^{ST}(\omega)\right)\right] \mathrm{d}\omega \tag{54}$$
$$\tag{55}$$

To complete the closed-form derivations, analytical expressions for $\bar{P}_L^{DA}(\omega)$, $\bar{P}_L^{ST}(\omega)$, $\bar{R}_L^{DA}(\omega)$, $\bar{R}_L^{ST}(\omega)$, $\bar{P}_V^{DA}(\omega)$, $\bar{P}_V^{ST}(\omega)$, $\bar{R}_V^{DA}(\omega)$ and $\bar{R}_V^{ST}(\omega)$ *spectral components* should be derived in terms of $P_L(\omega)$ and $P_V(\omega)$ normalized load and VER spectra. Since the cases for load and VER are calculated similarly, the derivation for only one profile is presented and the superscripts L, V are omitted.

TABLE II: Profile altering operations and their frequency domain representations

Operation	Definition	Frequency domain representation
Phase shifting by N samples	$P[n] = P_0[n-N]$	$P(\omega) = P_0(\omega)e^{-j\omega NT_s}$
Summing with N window	$P[n] = \sum_{k=0}^{N-1} P_0[n-k]$	$P(\omega) = P_0(\omega)\frac{1-e^{-j\omega NT_s}}{1-e^{-j\omega T_s}}$
Averaging with N window	$P[n] = \frac{1}{N}\sum_{k=0}^{N-1} P_0[n-k]$	$P(\omega) = P_0(\omega)\frac{1}{N}\frac{1-e^{-j\omega NT_s}}{1-e^{-j\omega T_s}}$
Downsampling with N step	$P[n] = \begin{cases} P_0[n], & n = k\cdot N; \\ 0, & \text{otherwise.} \end{cases}$	$P(\omega) = \frac{1}{N}\sum_{n=0}^{N-1} P_0\left(\omega - \frac{2\pi n}{NT_s}\right)$
Differencing with N step	$P[n] = \frac{P_0[n]-P_0[n-N]}{NT_s}$	$P(\omega) = \frac{1}{NT_s}P_0(\omega)\left(1-e^{-j\omega NT_s}\right)$

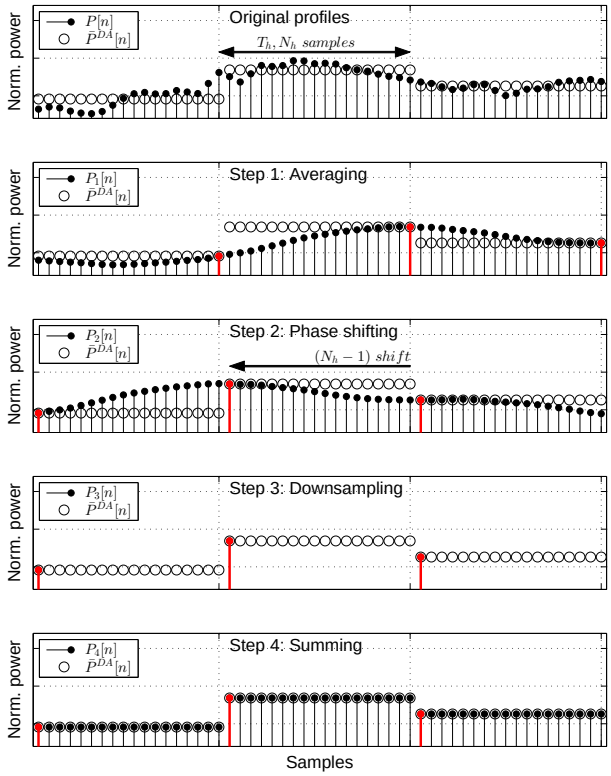

Fig. 6: Four steps of $\bar{P}^{DA}[n]$ determination

E. Determination of the spectral components

The goal now is to obtain analytical expressions for $\bar{P}^{DA}(\omega)$, $\bar{P}^{ST}(\omega)$, $\bar{R}^{DA}(\omega)$, $\bar{R}^{ST}(\omega)$ in terms of $P(\omega)$. This is done by using a set of linear operations presented in Table II along with their frequency domain representations. Applying these operations on $P(\omega)$ in particular orders generates the desired outputs. To make the idea behind the chosen sequence of the operations easier to grasp, the derivation steps are demonstrated in the time domain first and then projected into the frequency domain using the time–frequency mapping in Table II.

1) Determination of $\bar{P}^{DA}[n]$: To obtain $\bar{P}^{DA}[n]$, the following four operations are applied on $P[n]$ in the given order, also demonstrated in Fig. 6:

1) *Averaging with N_h window*
2) *Phase shifting by $N_h - 1$ samples*
3) *Downsampling with N_h step*
4) *Summing with N_h window*

The linearity of the operations allows their projection into the frequency domain. Using the time–frequency mapping of the operations in Table II and taking into account that $N_h T_s = T_h$, the final expression with incorporated variabilities takes the

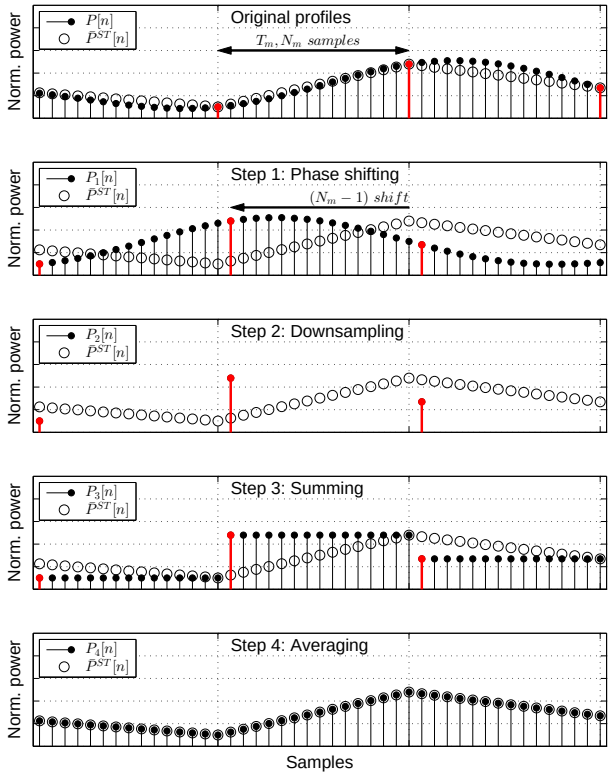

Fig. 7: Four steps of $\bar{P}^{ST}[n]$ determination

following form [12]:

$$\bar{P}^{DA}(\omega) = -\frac{1}{(\alpha T_h)^2} \sum_{n=-\infty}^{+\infty} \left[\frac{P\left(\omega - \frac{2\pi n}{\alpha T_h}\right)}{\omega - \frac{2\pi n}{\alpha T_h}} \right] \frac{\left(1 - e^{-j\omega\alpha T_h}\right)^2}{\omega} e^{j\omega\alpha T_h} \tag{56}$$

2) Determination of $\bar{P}^{ST}[n]$: Similarly, $P^{ST}[n]$ is obtained by applying the same operations on $P[n]$ in a slightly different order as demonstrated in Fig. 7:

1) *Phase shifting by $N_m - 1$ samples*
2) *Downsampling with N_m step*
3) *Summing with N_m window*
4) *Averaging with N_m window*

The linearity of the operations allows their projection into the frequency domain. Using the time–frequency mapping of the operations in Table II and taking into account that $N_m T_s = T_m$, the final expression with incorporated variabilities takes the following form [14]:

$$\bar{P}^{ST}(\omega) = -\frac{1}{(\alpha T_m)^2} \sum_{n=-\infty}^{+\infty} \left[P\left(\omega - \frac{2\pi n}{\alpha T_m}\right) \right] \frac{\left(1 - e^{-j\omega\alpha T_m}\right)^2}{\omega^2} e^{j\omega\alpha T_m} \tag{57}$$

3) Determination of $\bar{R}^{DA}[n]$: $\bar{R}^{DA}[n]$ is obtained by applying the following five operations on $P[n]$, also demonstrated in Fig. 8:

1) *Averaging with N_h window*
2) *Phase shifting by $N_h - 1$ samples*
3) *Downsampling with N_h step*
4) *Differencing with N_h step*
5) *Summing with N_h window*

The linearity of the operations allows their projection into the frequency domain. Using the time–frequency mapping of the operations in Table II and taking into account that $N_h T_s = T_h$, the final expression with incorporated variabilities takes the following form [13]:

$$\bar{R}^{DA}(\omega) = \frac{1}{(\alpha T_h)^3} \cdot \sum_{n=-\infty}^{+\infty} \left[\frac{P\left(\omega - \frac{2\pi n}{\alpha T_h}\right)}{\omega - \frac{2\pi n}{\alpha T_h}} \right] \frac{\left(1 - e^{-j\omega\alpha T_h}\right)^3}{-\omega} e^{j\omega\alpha T_h} \tag{58}$$

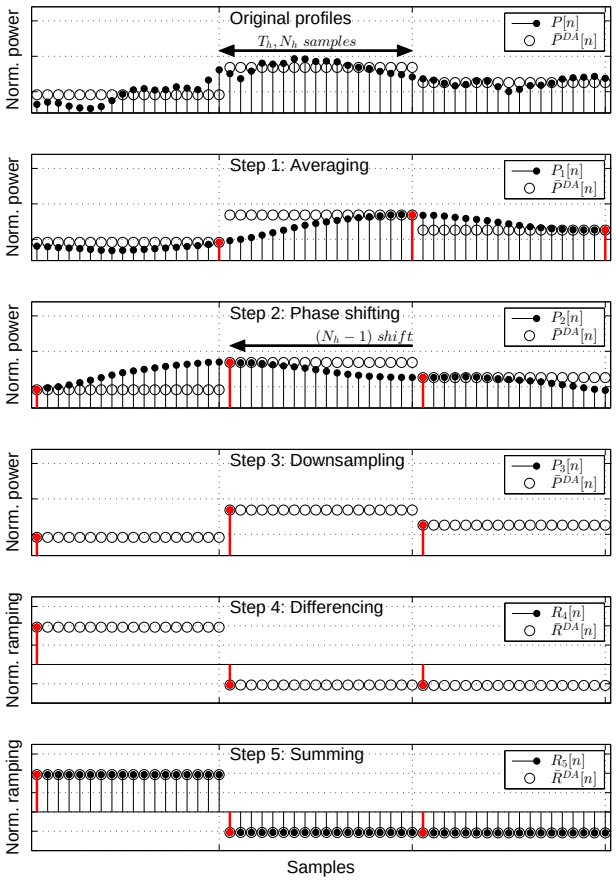

Fig. 8: Five steps of $\bar{R}^{DA}[n]$ determination

4) Determination of $\bar{R}^{ST}[n]$: To obtain $\bar{R}^{ST}[n]$, the following four operations are applied on $P[n]$ in the given order, also demonstrated in Fig. 9:

1) *Phase shifting by $N_m - 1$ samples*
2) *Downsampling with N_m step*
3) *Differencing with N_m step*
4) *Summing with N_m window*

The linearity of the operations allows their projection into the frequency domain. Using the time–frequency mapping of the operations in Table II and taking into account that $N_m T_s = T_m$, the final expression with incorporated variabilities takes the following form:

$$\bar{R}^{ST}(\omega) = \frac{1}{(\alpha T_m)^2} \sum_{n=-\infty}^{+\infty} \left[P\left(\omega - \frac{2\pi n}{\alpha T_m}\right) \right] \frac{\left(1 - e^{-j\omega\alpha T_m}\right)^2}{j\omega} e^{j\omega\alpha T_m} \tag{59}$$

Thus, the standard deviations of mismatch terms can be obtained by substituting spectral expressions (56)–(59) into (52)–(54). It should be noted that $P(\omega)$ spectrum in (56)–(59) is the net of spatial variation.

To summarize, equations (56)–(59) take the normalized load and VER spectra as inputs, along with principal parameters. It is known from the literature, that both load and VER power spectra has distinctive shapes that tend to remain consistent for different cases [41], [42]. As a result, the normalized load and VER spectra can be obtained once for a given case and used in the calculations of the reserve requirements for different cases. Thus, the operating reserve requirements for a particular case can be calculated *a priori*, without prior knowledge of load and VER time domain profiles for that particular case. Next, the values of $\bar{P}_{DA}(\omega)$, $\bar{P}_{ST}(\omega)$, $\bar{R}_{DA}(\omega)$, $\bar{R}_{ST}(\omega)$ calculated from (56)–(59) respectively are substituted into (52)–(54) to obtain $\left(\sigma_\alpha^{LF}\right)_{XY}$, $\left(\sigma_\alpha^{RP}\right)_{XY}$, $\left(\sigma_\alpha^{RG}\right)_{XY}$. Then, the standard deviations of the mismatch terms are calculated from (43)–(48). Finally, the operating reserve requirements are determined according to (27)–(29).

IV. Numerical validation

The proposed methodology is numerically validated for different scenarios of power system operations. The actual load and VER profiles for each scenario are modeled according to (33) and (34) respectively, using different sets of principal parameters.

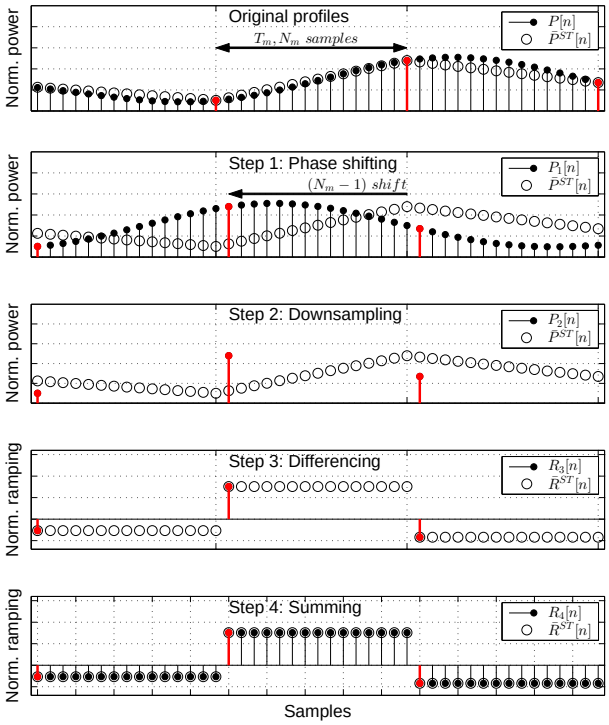

Fig. 9: Four steps of $\bar{R}^{ST}[n]$ determination

TABLE III: Numerical validation scenarios for different values of principal parameters

Scenario	$T_h(min)$	$T_m(min)$	π	α_L, α_V	ε_V^{DA}	ε_V^{ST}
A1	60	5	0	1	0	0
A2	30	5	0	1	0	0
A3	15	5	0	1	0	0
B1	60	10	0	1	0	0
B2	60	15	0	1	0	0
B3	60	30	0	1	0	0
C1	60	5	0.05	1	0	0
C2	60	5	0.1	1	0	0
C3	60	5	0.2	1	0	0
D1	60	5	0.2	2	0	0
D2	60	5	0.2	3	0	0
D3	60	5	0.2	4	0	0
E1	60	5	0.2	1	0.02	0
E2	60	5	0.2	1	0.05	0
E3	60	5	0.2	1	0.1	0
F1	60	5	0.2	1	0	0.01
F2	60	5	0.2	1	0	0.02
F3	60	5	0.2	1	0	0.05

The normalized load and wind data in (33) and (34) are obtained from Bonneville Power Administration (BPA) repositories [43]. To cover as many different combinations as possible, each parameter is varied for three different values. The load and VER variabilities are changed together so as to change the total variability of the net load. Since the load and VER forecast errors appear as a sum in (49)–(51), it is sufficient to conduct the numerical validation for only one type of error and, therefore, the day–ahead and the short–term forecast errors of the load are set to zero. This helps to reduce the total number of scenarios to 18, divided into six subsets as presented in Table III. The load following, ramping and regulation reserve requirements for each scenario are calculated according to (27)–(29) respectively. The validation process for each scenario is two–fold. It tests both the accuracy of the calculations and the balancing performance of the power system when the reserve requirements are calculated by the proposed methodology.

TABLE IV: The accuracy of the operating reserve requirement calculation and the balancing performance of the system for each scenario

Scenario	P^{LF} $(\times 10^{-3})$	P_0^{LF} $(\times 10^{-3})$	Accuracy	Performance	R^{RP} $(\times 10^{-4})$	R_0^{RP} $(\times 10^{-4})$	Accuracy	Performance	P^{RG} $(\times 10^{-4})$	P_0^{RG} $(\times 10^{-4})$	Accuracy	Performance
A1	13.2126	13.2249	99.91%	91.03%	16.0545	16.1222	99.58%	93.45%	–	–	–	–
A2	7.7751	7.7894	99.82%	91.14%	15.6662	15.7313	99.59%	93.17%	–	–	–	–
A3	4.7561	4.7750	99.61%	90.27%	15.5063	15.5541	99.69%	93.11%	–	–	–	–
B1	13.0690	13.0806	99.91%	91.51%	9.8342	9.8518	99.82%	93.67%	16.8120	16.8143	99.99%	91.99%
B2	13.0932	13.1055	99.91%	90.67%	7.5430	7.5495	99.91%	93.42%	52.7228	52.7237	99.99%	92.29%
B3	13.3725	13.3867	99.89%	90.64%	5.0298	5.0277	99.96%	92.15%	69.4704	69.4601	99.99%	92.55%
C1	13.2735	13.2858	99.91%	90.04%	16.0748	16.1424	99.58%	93.44%	16.8095	16.8118	99.99%	91.98%
C2	13.4775	13.4898	99.91%	90.93%	16.1993	16.2669	99.59%	93.06%	17.0343	16.8596	99.99%	91.98%
C3	14.2860	14.2984	99.91%	91.86%	16.7501	16.8172	99.60%	92.52%	17.1012	17.1039	99.99%	91.88%
D1	26.4843	26.5110	99.90%	91.94%	22.8982	22.9659	99.70%	92.80%	43.8151	43.8300	99.97%	92.04%
D2	36.9023	36.9368	99.91%	90.32%	30.6761	30.7370	99.80%	92.27%	54.0845	54.0900	99.99%	91.93%
D3	51.2782	51.3405	99.88%	90.55%	39.6784	39.7154	99.90%	92.04%	61.7933	61.7988	99.99%	91.86%
E1	15.7537	15.7667	99.92%	90.67%	16.7575	16.8335	99.55%	92.59%	–	–	–	–
E2	21.9009	21.9190	99.92%	90.91%	16.7971	16.8862	99.47%	92.53%	–	–	–	–
E3	36.1432	36.1741	99.91%	90.42%	16.9377	17.0485	99.35%	92.63%	–	–	–	–
F1	–	–	–	–	–	–	–	–	39.2153	39.0434	99.56%	92.04%
F2	–	–	–	–	–	–	–	–	72.6222	72.4576	99.77%	91.86%
F3	–	–	–	–	–	–	–	–	177.2767	177.1738	99.94%	91.77%

A. Accuracy of the calculations

While time and frequency domain representations of the equations are identical and carry exactly the same information, the final forms of the spectral components (56)–(59) are obtained by using several simplifying approximations, as discussed in detail in [12], [13], [14]. Thus, it is important to study how those approximations alter the accuracy of the operating reserve requirements calculations. To achieve that, the reserve requirements calculated using the spectral components (56)–(59) $\left(P^{LF}, R^{RP}, P^{RG}\right)$, are compared to the reserve requirements calculated from the original unaltered time domain data, by calculating the standard deviations of the mismatch terms (37), (38), (39) $\left(P_0^{LF}, R_0^{RP}, P_0^{RG}\right)$.

B. Balancing performance of the power system

The goal of the proposed methodology is to calculate the reserve requirements that keep the balancing performance of the power system in accordance with the NERC requirements, where the balancing performance is defined as the percentage of time the dispatched generation is able to meet the real–time demand. To verify whether the proposed methodology achieves this goal, the power system operations are simulated for one year period for the scenarios listed in Table III. This study uses the power system enterprise control simulator introduced in [31], [32], that models the power system operations as a multi–layer control hierarchy on top of the physical power grid. The control hierarchy consists of three layers, namely resource scheduling, balancing actions and regulation service, as briefly described in Section II-B and presented in Fig. 2. As in previous work on power grid enterprise control [31], [32], and earlier work on operating reserve requirements [12], [13], [14], the simulator uses the physical power grid data from IEEE reliability test system RTS–96, consisting of 73 buses and 99 generation units [44]. The goal is to test whether the balancing performance of the power system meets NERC required 90% minimum value when the load following, ramping and regulation reserve requirements are calculated according to (27)–(29) respectively, and β^{LF}, β^{RP}, β^{RG} are taken equal to (40)–(42) respectively.

C. Validation results

The validation results are presented in Table IV, where the reserve amounts are normalized by the system peak load P_L^{peak}. The accuracy is defined as the relative difference between P^{LF}, R^{RP}, P^{RG} and $P_0^{LF}, R_0^{RP}, P_0^{RG}$ values respectively. The results clearly show, that the implemented simplifications have negligible impact on the accuracy of calculations. All differences between the two compared values are less than 1%.

The balancing performance of the power system for each scenario is also shown in Table IV, where the reserve requirements are calculated according to (27)–(29). The results indicate that the balancing performance exceeds the NERC required 90% threshold for all scenarios. The fact, that the performance exceeds the required threshold slightly only, indicates that the calculation of the reserve requirements is neither undersized nor oversized. Combined with the calculation accuracy tests, these results validate the proposed methodology.

In summary, the proposed methodology is validated for a wide range of power system operation scenarios. The validation results show that the proposed methodology is able to calculate the operating reserve requirements with sufficiently high accuracy. Also, the operating reserve requirements calculated from (27)–(29) keep the system in compliance with NERC balancing requirements. Such an *a priori* reserve requirement calculation methodology can have a variety of applications in power system operations and planning. One of such applications is assessment of the VER penetration impact on the power system operating reserve requirements for different scenarios, which is addressed in the following section.

It is important to note that the proposed method for determining the required quantities of operating reserves does not consider network constraints. Nevertheless, it is understood that these operating reserves, once sized, would be deployed within well-known security constrained unit commitment (SCUC) and security constrained economic dispatch (SCED) optimizations (as in [31], [32]); thus respecting the spatial distribution of forecasted net loads in normal operation. In the event that the network experiences a significantly different spatial distribution of net loads than forecasted, causing a limitation on the deployment of (normal) operating reserves, then a contingency would be raised. In such a case, using the adopted classification of reserves found in [26], [27], contingency reserves (mentioned as outside of the scope of this paper in Section II-B), would need to be deployed.

V. Sensitivity analysis of the operating reserve requirements to the net load and power system parameters

The intermittent nature of VER brings new challenges to the power system reliable operations. To that end, an extensive academic and industrial literature has developed to study the impact of such VER integration on different aspects of power system operations [45], [46], [47]. While most of these studies agree that VER integration increases the power system reserve requirements, the conclusions about the impact size diverge [23], [26], [27], [48], [49], [50]. These discrepancies in the results can be attributed to the use of different methodologies, analysis tools and historical data [51], [52]. Moreover, while VER variability and forecast error have different impact mechanisms on reserve requirements, most of these studies do not distinguish them and consider either their combined impact or the discussion is limited to only one of them as discussed above. As a result, the sensitivity of the reserve requirement to each parameter becomes harder to assess. However, the major limitation of these studies is the use of *a posteriori* assessment methods that are only valid if the environment of the power system operations is unchanged. As a result, possible changes of the power system operating conditions (e.g., scheduling time step or VER variability) make the results of such methods void.

In this section, the developed operating reserve determination methodology is used to analyze the sensitivity of each type of reserve requirements to the net load and power system parameters, which is an essential part of describing how the VER integration affects the reserve requirements and helps to better accommodate the VER in power systems. A similar study has used a simulation-based methodology to *assess* the sensitivity of the reserve requirements to the principal parameters for few simulation results [31], [32]. In contrast, the explicit analytical expressions presented in here reveal the functional forms of the sensitivities and allow decomposing the combined impact of these parameters into *ceteris paribus* scenarios. To achieve this goal, the following five aspects are studied for each type of reserves:

- *The impact of the VER variability α_V on operating reserve requirements*
- *The impact of the VER day–ahead forecast error ε_V^{DA} on operating reserve requirements*
- *The impact of the VER short–term forecast error ε_V^{ST} on operating reserve requirements*
- *The impact of the scheduling time step T_h on operating reserve requirements*
- *The impact of the balancing time step T_m on operating requirements*

Since the focus of this study is the impact of VER integration, the variability and forecast errors of load are set to constant values at $\alpha_L = 1$ and $\varepsilon_L^{DA} = \varepsilon_L^{ST} = 0$ respectively. Moreover, since the capacity factor γ appears only as a multiplier to penetration level π, it is of a small interest for this study and is also omitted. For each scenario, the dependence curves of each type of reserve requirement on the VER penetration level is constructed for three different values of the corresponding parameter. Load and wind data for one year from Bonneville Power Administration (BPA) repositories [43] are used for this study.

A. Sensitivity analysis of the load following reserve requirement

As discussed above, the variability and the forecast error are the two parameters that affect the VER induced power system load following reserve requirement. The wind forecast error is set to zero for the first scenario to make the impact of variability more visible. The results in Fig. 10 show, that high VER variability significantly increases the load following reserve requirement. For $\alpha_V = 3$, the load following reserve requirement increases by $\sim 50\%$ compared to the case without VER as the penetration level reaches 20%. Similarly, the results in Fig. 11 show, that the presence of the day–ahead forecast error also increases the load following reserve requirement. However, unlike the variability, the impact of the day–ahead forecast error is much higher. For a reasonable 10% forecast error, the load following reserve requirement more than doubles as wind penetration level reaches 20%. Thus, both the VER variability and the VER day–ahead forecast error lead to significant increase of the load following reserve requirement. It is important to notice, that the impact of the forecast error for the given penetration scenario can only be mitigated by improving the forecasting accuracy, since, according to (49), σ_ε^{LF} only depends on the day–ahead forecast error and penetration level. On the other hand, the dependence of (56)–(57) on T_h and T_m respectively suggests that the impact of the variability can be altered by changing these parameters.

To that end, the impact of the scheduling and the balancing time steps on the load following reserve requirement is simulated. The results in Fig. 12 show that reduction of the scheduling time step drops the reserve requirement significantly. This is due to the fact that the scheduling time step and the variability always appear as multipliers in (56), and, hence, have identical impact on the reserve requirement. However, as the penetration level increases, the relative improvement diminishes as the

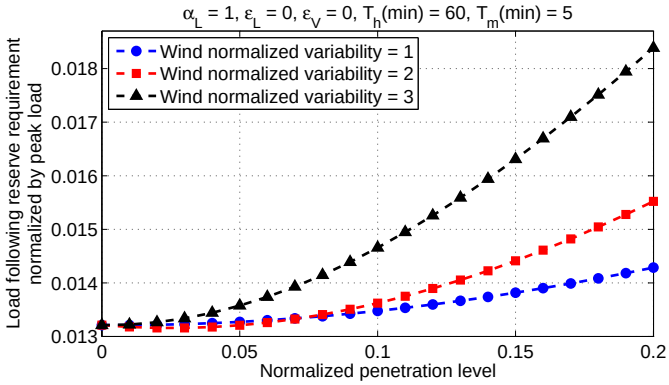

Fig. 10: Increase of load following reserve requirement for wind penetration with different variabilities

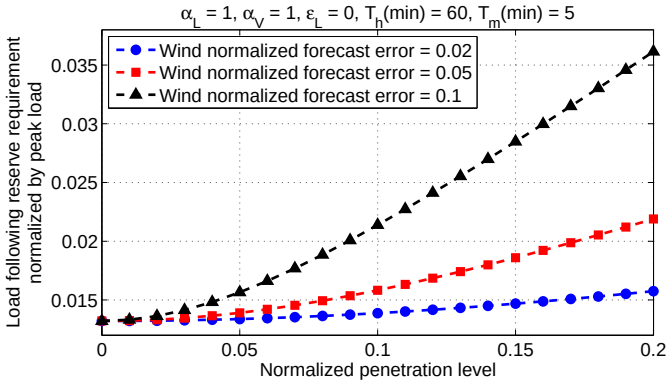

Fig. 11: Increase of load following reserve requirement for wind penetration with different day-ahead forecast errors

impact of the day–ahead forecast error dominates. On the other hand, the results in Fig. 13 show that the balancing time step has a negligible impact on the load following reserve requirement.

In summary, both VER variability and VER day–ahead forecast error can increase the load following reserve requirement significantly. While the impact of the forecast error can only be alleviated by improving the forecasting accuracy, the impact of the variability can be effectively mitigated by reducing the scheduling time step. Although the impact of the balancing time step on the load following reserve requirement is negligible, its small value is preferable since it reduces the ramping and regulation reserve requirements as shown below. Thus, improved forecasting accuracy and shorter scheduling time step are able to mitigate the burden of VER integration on the load following reserve requirement.

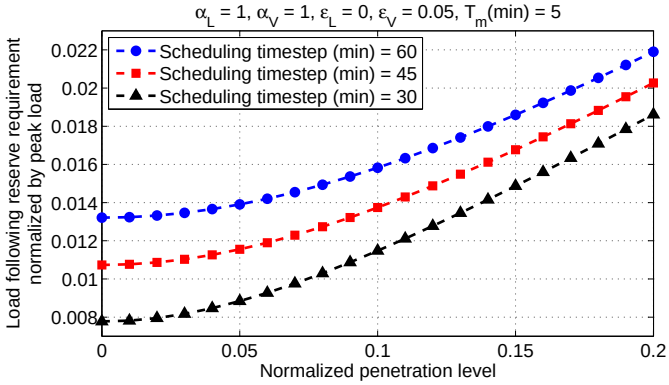

Fig. 12: Increase of load following reserve requirement for wind penetration into the system with different scheduling time steps

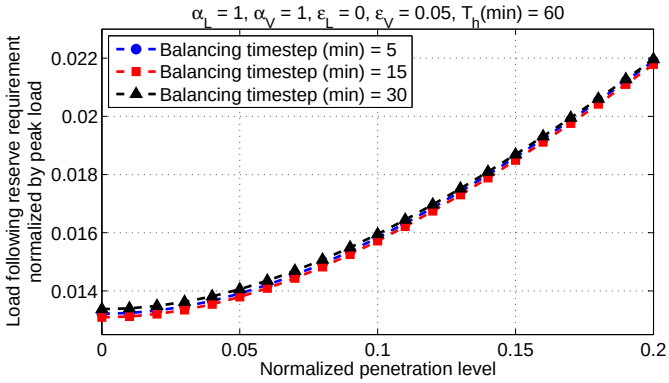

Fig. 13: Increase of load following reserve requirement for wind penetration into the system with different balancing time steps

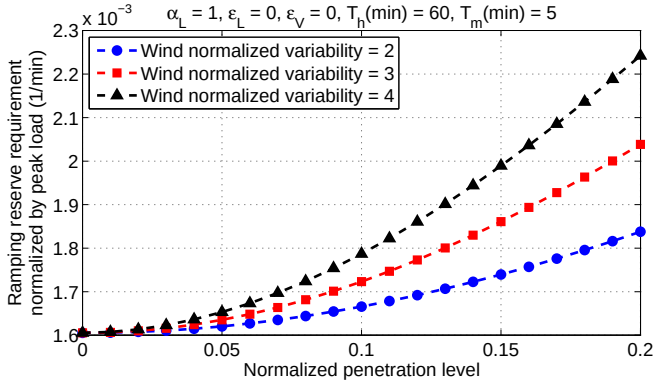

Fig. 14: Increase of ramping reserve requirement for wind power penetration with different variabilities

B. Sensitivity analysis of the ramping reserve requirement

As discussed above, the variability and the forecast error are the two parameters that may affect the VER induced power system ramping reserve requirement. The wind forecast error is set to zero for the first scenario to make the impact of the variability more visible. The results in Fig. 14 show, that high VER variability significantly increases the ramping reserve requirement. For $\alpha_V = 4$, the ramping reserve requirement increases by $\sim 50\%$ as the penetration level reaches 20% compared to the case without VER. In contrast, the results in Fig. 15 show, that the day–ahead forecast error has comparably modest impact on the ramping reserve requirement. Even for a 10% day-ahead forecast error, the increase of the ramping reserve requirement is only marginal for 20% wind penetration. It is also important to notice, that according to (50), the impact of the day–ahead forecast error for the given penetration level can only be mitigated by improving the forecasting accuracy. On the other hand, the dependence of (58)–(59) on T_h and T_m respectively suggests that the impact of the variability can be altered by changing these parameters.

To that end, the impact of the scheduling and the balancing time steps on the ramping reserve requirement is studied. The

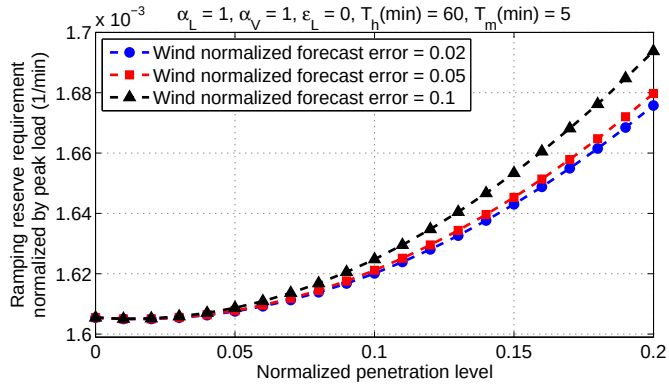

Fig. 15: Increase of ramping reserve requirement for wind power penetration with different day-ahead forecast errors

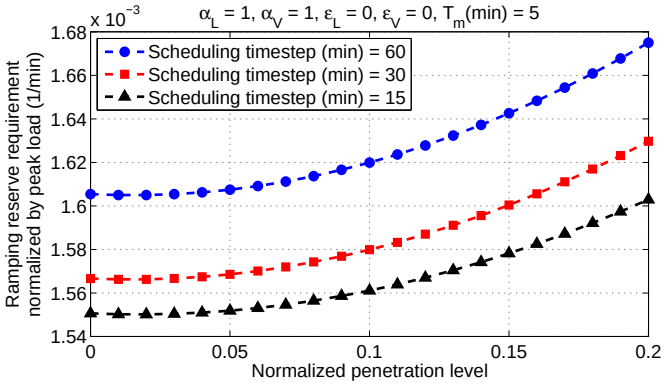

Fig. 16: Increase of ramping reserve requirement for wind power penetration in the case of different scheduling time steps

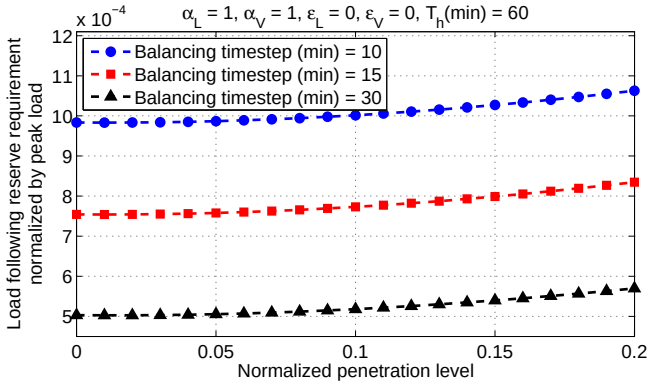

Fig. 17: Increase of ramping reserve requirement for wind power penetration in the case of different balancing time steps

results in Fig. 16 show that reducing the scheduling time step reduces the ramping reserve requirement only slightly. On the other hand, the results in Fig. 17 show that the impact of balancing time step on the ramping reserve requirement is significant. Increase of the balancing time step can drop the ramping reserve requirement of the system with VER integration even below the requirement the system had before wind integration.

In summary, highly variable VER penetration increases the ramping reserve requirement. While the moderate impact of the day–ahead forecast error can only be alleviated by improving the forecasting accuracy, the more significant impact of the variability can be effectively mitigated by increasing the balancing time step. Although the impact of the scheduling time step on the ramping reserve requirement is negligible, its small value is preferable since it reduces the load following reserve requirement as established above. Thus, improved forecast accuracy and longer balancing time step are able to mitigate the burden of VER integration on the ramping reserve requirement.

C. Sensitivity analysis of the regulation reserve requirement

As discussed above, the variability and the forecast error are the two parameters that affect the VER induced power system regulation reserve requirement. For the first scenario, the wind forecast error is set to zero to highlight the impact of the VER variability. The results in Fig. 18 show, that high VER variability significantly increases the regulation reserve requirement. For $\alpha_V = 4$, the regulation reserve requirement increases by $\sim 50\%$ as the penetration level reaches 20% compared to the case without VER. Similarly, the results in Fig. 19 show, that the presence of the short–term forecast error also increases the regulation reserve requirement. However, unlike the variability, the impact of the short-term forecast error is much higher. For a reasonable 2% short–term forecast error, the regulation reserve requirement more than triples as wind penetration level reaches 20%. Thus, both the VER variability and the VER short-term forecast error lead to significant increase of the regulation reserve requirement. Also, according to (51), the impact of the forecast error for the given penetration level can only be mitigated by improving the forecasting accuracy. In contrast, the dependence of (57) on T_m suggests that the impact of the variability can be altered by changing the balancing time step.

Thus, it can be concluded that the short–term forecast error is the most significant factor defining the regulation reserve requirement. Starting at some wind penetration level, this dependence even turns linear, which indicates that the value of σ_α^{LF} in (30) becomes negligible compared to σ_ε^{LF}. This outcome can be considered as “unfortunate”, since the impact of the forecast error on the reserve requirements in general is more permanent than the impact of the variability. According to (56), the balancing time step and the variability always appear as multipliers, and thus have identical impact on the regulation reserve

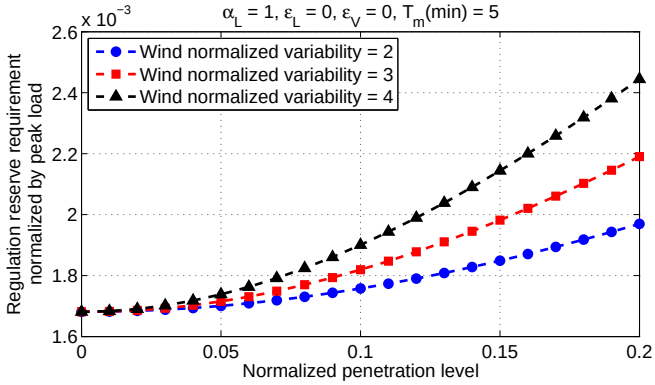

Fig. 18: Increase of regulation reserve requirement for wind power penetration with different variabilities

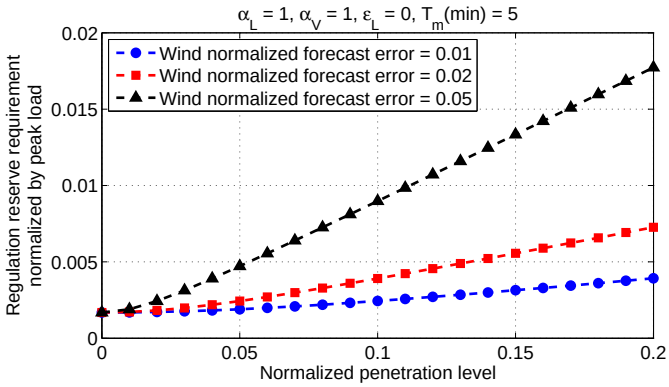

Fig. 19: Increase of regulation reserve requirement for wind power penetration with different short-term forecast errors

requirement. This suggests that the impact of wind variability on the regulation reserve requirement case can be effectively mitigated by manipulating the balancing time step. The results in Fig. 20 show that the reduction of the balancing time step can drop the regulation reserve requirement of the system with wind integration even below the requirement the system had before wind integration.

In summary, both VER variability and VER short–term forecast error can increase the regulation reserve requirement significantly. While the impact of the forecast error can only be alleviated by improving the forecasting accuracy, the impact of the variability can be effectively mitigated by reducing the balancing time step. Thus, improved forecasting accuracy and shorter balancing time step are able to mitigate the burden of VER integration on the regulation reserve requirement.

While the results of this paper are produced assuming reserve requirements assessment static approach, the proposed methodology can also be successfully applied to the dynamic case. The mathematical operations used to calculate reserve requirements, such as standard deviation and Fourier transform, produce averaged statistical characteristics of the input data. As a result, the reserve requirements assessed by these methods correspond to the averaged dynamics of the whole data. This

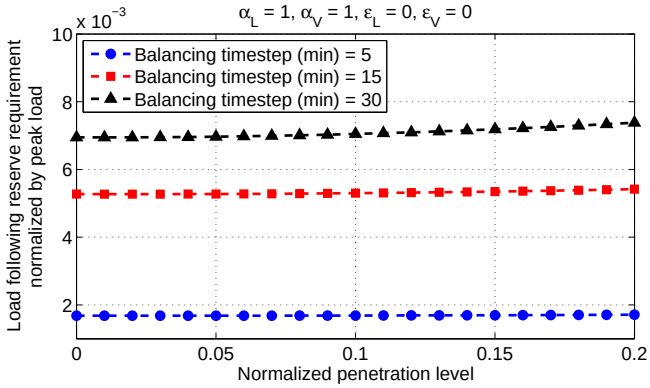

Fig. 20: Increase of regulation reserve requirement for wind power penetration in the case of different balancing time steps

approach might be inefficient, considering that the dynamics of the input data and the grid conditions may change from one period to another. The idea of a dynamic approach is breaking the available data into smaller time intervals corresponding to different data dynamics and grid conditions. This allows assessment of reserve requirements that are specifically adjusted for each time interval, which is likely to result in more efficient use of reserves. The proposed methodology can be used in a dynamic setup by breaking the input data into smaller intervals and calculating the power spectra and, therefore, the reserve requirements for each interval separately. The choice of the interval size depends on how specifically the reserve requirements should represent each interval and can be as small as needed, provided there is enough data to produce meaningful power spectra for each interval.

VI. Conclusion

This paper is an extension to the operating reserve requirement calculation methodology published previously [12], [13], [14]. The findings of the previous work are extended by the following three contributions. First, the methodology is generalized to also include the dependence of the load following and ramping reserve requirements on the balancing time step. Second, a comprehensive numerical validation of the methodology is performed by a set of extensive simulations that test both the accuracy of the calculations and the balancing performance of the power system. Third, the sensitivity of each type of reserve requirement to the net load and power system parameters is studied. The results show that increased VER variability can significantly increase all three types of reserve requirements. Also, while the impact of the forecast error on the ramping reserve requirement is negligible, its impact on the load following and regulation reserve requirements can dominate that of the variability. On the other hand, reducing the day-ahead scheduling time-step is able to mitigate the impact of the variability on the load following reserve requirement while has negligible impact on the ramping and regulation reserve requirements. Also, changing the balancing time step has no noticeable impact on the load following reserve requirement, while it has opposing impacts on the ramping and regulation reserve requirements. Reducing the balancing time step reduces the regulation reserve requirement but increases the ramping reserve requirement.

Appendix: Derivations of the mismatch terms

This appendix presents the derivations of the mismatch term expressions (37)–(39). Load and VER models (33)–(36) are used to explicitly incorporate the principal parameters into the mismatch terms (21)–(23). Besides the actual load and VER profiles, these models can also be applied to the auxiliary profiles in Definitions 12–18. In the further derivations, the superscript '0' is omitted for clarity.

$\Delta P^{DA}(t)$ *mismatch term*

The best day–ahead forecast profile (14) is used to split the mismatch term (21) into two components:

$$\Delta P^{DA}(t) = \bar{P}^{ST}(t) - \hat{P}^{DA}(t) = \left(\bar{P}^{ST}(t) - \bar{P}^{DA}(t)\right) + \left(\bar{P}^{DA}(t) - \hat{P}^{DA}(t)\right) = \Delta P^{DA}_{\alpha}(t) + \Delta P^{DA}_{\varepsilon}(t) \tag{60}$$

Each components is studied separately. Using (33) and (34), $\Delta P^{DA}_{\alpha}(t)$ can be written as:

$$\begin{aligned}\Delta P^{DA}_{\alpha}(t) = \bar{P}^{ST}(t) - \bar{P}^{DA}(t) = \left(\bar{P}^{ST}_{L}(t) - \bar{P}^{DA}_{L}(t)\right) - \left(\bar{P}^{ST}_{V}(t) - \bar{P}^{DA}_{V}(t)\right) = \\ = \left(\left(\bar{p}^{ST}_{L}(\alpha_L t) - \bar{p}^{DA}_{L}(\alpha_L t)\right) - \gamma\cdot\pi\cdot\left(\bar{p}^{ST}_{V}(\alpha_V t) - \bar{p}^{DA}_{V}(\alpha_V t)\right)\right)\cdot P^{peak}_{L}\end{aligned} \tag{61}$$

Next, $\Delta P^{DA}_{\varepsilon}(t)$ is represented as follows:

$$\begin{aligned}\Delta P^{DA}_{\varepsilon}(t) = \left(\bar{P}^{DA}(t) - \hat{P}^{DA}(t)\right) = \left(\bar{P}^{DA}_{L}(t) - \hat{P}^{DA}_{L}(t)\right) - \left(\bar{P}^{DA}_{V}(t) - \hat{P}^{DA}_{V}(t)\right) = \\ = \left(\frac{\bar{P}^{DA}_{L}(t) - \hat{P}^{DA}_{L}(t)}{\mathrm{std}\left(\bar{P}^{DA}_{L}(t) - \hat{P}^{DA}_{L}(t)\right)}\cdot\frac{\mathrm{std}\left(\bar{P}^{DA}_{L}(t) - \hat{P}^{DA}_{L}(t)\right)}{P^{peak}_{L}} - \frac{\bar{P}^{DA}_{V}(t) - \hat{P}^{DA}_{V}(t)}{\mathrm{std}\left(\bar{P}^{DA}_{V}(t) - \hat{P}^{DA}_{V}(t)\right)}\cdot\frac{\mathrm{std}\left(\bar{P}^{DA}_{V}(t) - \hat{P}^{DA}_{V}(t)\right)}{P^{max}_{V}}\cdot\frac{P^{max}_{V}}{P^{peak}_{L}}\right)\cdot P^{peak}_{L}\end{aligned} \tag{62}$$

Equation (62) contains identical expressions in form of standard deviations for load and VER profiles. Thus, it is calculated only once and the subscripts L,V are omitted [12]:

$$\begin{aligned}\left[\mathrm{std}\left(\bar{P}^{DA}(t) - \hat{P}^{DA}(t)\right)\right]^2 = \frac{1}{T}\int_0^T\left(\bar{P}^{DA}(t) - \hat{P}^{DA}(t)\right)^2\mathrm{dt} = \frac{1}{nT_h}\int_0^{nT_h}\left(\bar{P}^{DA}(t) - \hat{P}^{DA}(t)\right)^2\mathrm{dt} = \\ = \frac{1}{n}\sum_{k=0}^{n-1}\frac{1}{T_h}\int_{kT_h}^{(k+1)T_h}\left(\bar{P}^{DA}(t) - \hat{P}^{DA}(t)\right)^2\mathrm{dt} = \frac{1}{n}\sum_{k=0}^{n-1}\left(\bar{P}^{DA}[k] - \hat{P}^{DA}[k]\right)^2\end{aligned} \tag{63}$$

Thus, using the definitions of load and VER forecast errors (9) and (10) respectively, and the definition of the VER penetration level (1), (62) can be written as:

$$\Delta P_{\varepsilon}^{DA}(t) = \left(\varepsilon_L^{DA} \cdot \xi_L^{DA}(t) - \varepsilon_V^{DA} \cdot \pi \cdot \xi_V^{DA}(t)\right) \cdot P_L^{peak} \tag{64}$$

where $\xi_L^{DA}(t)$ and $\xi_V^{DA}(t)$ are load and VER day–ahead forecast error time series respectively, normalized to unit standard deviations. Thus, substituting (61) and (64) into (60), the mismatch term (21) takes the following form:

$$\Delta P^{DA}(t) = \left(\left(\bar{p}_L^{ST}(\alpha_L t) - \bar{p}_L^{DA}(\alpha_L t)\right) - \gamma \cdot \pi \cdot \left(\bar{p}_V^{ST}(\alpha_V t) - \bar{p}_V^{DA}(\alpha_V t)\right) + \varepsilon_L^{DA} \cdot \xi_L^{DA}(t) - \varepsilon_V^{DA} \cdot \pi \cdot \xi_V^{DA}(t)\right) \cdot P_L^{peak} \tag{65}$$

$\Delta R^{DA}(t)$ mismatch term

The best day–ahead ramping forecast profile (18) is used to split the mismatch term (22) into two components:

$$\Delta R^{DA}(t) = \bar{R}^{ST}(t) - \hat{R}^{DA}(t) = \left(\bar{R}^{ST}(t) - \bar{R}^{DA}(t)\right) + \left(\bar{R}^{DA}(t) - \hat{R}^{DA}(t)\right) = \Delta R_{\alpha}^{DA}(t) + \Delta R_{\varepsilon}^{DA}(t) \tag{66}$$

Each components is studied separately. Using (35) and (36), $\Delta R_{\alpha}^{DA}(t)$ can be written as:

$$\begin{aligned}\Delta R_{\alpha}^{DA}(t) = \bar{R}^{ST}(t) - \bar{R}^{DA}(t) = \left(\bar{R}_L^{ST}(t) - \bar{R}_L^{DA}(t)\right) - \left(\bar{R}_V^{ST}(t) - \bar{R}_V^{DA}(t)\right) = \\ = \left(\alpha_L \cdot \left(\bar{r}_L^{ST}(\alpha_L t) - \bar{r}_L^{DA}(\alpha_L t)\right) - \alpha_V \cdot \gamma \cdot \pi \cdot \left(\bar{r}_V^{ST}(\alpha_V t) - \bar{r}_V^{DA}(\alpha_V t)\right)\right) \cdot P_L^{peak}\end{aligned} \tag{67}$$

Next, $\Delta R_{\varepsilon}^{DA}(t)$ is represented as follows:

$$\begin{aligned}\Delta R_{\varepsilon}^{DA}(t) = \left(\bar{R}^{DA}(t) - \hat{R}^{DA}(t)\right) = \left(\bar{R}_L^{DA}(t) - \hat{R}_L^{DA}(t)\right) - \left(\bar{R}_V^{DA}(t) - \hat{R}_V^{DA}(t)\right) = \\ = \left(\frac{\bar{R}_L^{DA}(t) - \hat{R}_L^{DA}(t)}{\mathrm{std}\left(\bar{R}_L^{DA}(t) - \hat{R}_L^{DA}(t)\right)} \cdot \frac{\mathrm{std}\left(\bar{R}_L^{DA}(t) - \hat{R}_L^{DA}(t)\right)}{P_L^{peak}} - \frac{\bar{R}_V^{DA}(t) - \hat{R}_V^{DA}(t)}{\mathrm{std}\left(\bar{R}_V^{DA}(t) - \hat{R}_V^{DA}(t)\right)} \cdot \frac{\mathrm{std}\left(\bar{R}_V^{DA}(t) - \hat{R}_V^{DA}(t)\right)}{P_V^{max}} \cdot \frac{P_V^{max}}{P_L^{peak}}\right) \cdot P_L^{peak}\end{aligned} \tag{68}$$

Equation (68) contains identical expressions in form of standard deviations for load and VER ramping rates. Thus, it is calculated only once and the subscripts L,V are omitted [13]:

$$\begin{aligned}&\left[\mathrm{std}\left(\bar{R}^{DA}(t) - \hat{R}^{DA}(t)\right)\right]^2 = \frac{1}{T}\int_0^T \left(\bar{R}^{DA}(t) - \hat{R}^{DA}(t)\right)^2 \mathrm{dt} = \frac{1}{nT_h}\int_0^{nT_h} \left(\bar{R}^{DA}(t) - \hat{R}^{DA}(t)\right)^2 \mathrm{dt} = \frac{1}{n}\sum_{k=0}^{n-1}\frac{1}{T_h}\int_{kT_h}^{(k+1)T_h} \left(\bar{R}^{DA}(t) - \hat{R}^{DA}(t)\right)^2 \mathrm{dt} = \\ &= \frac{1}{n}\sum_{k=0}^{n-1}\left(\bar{R}^{DA}[k] - \hat{R}^{DA}[k]\right)^2 = \frac{1}{nT_h^2}\sum_{k=0}^{n-1}\left[\left(\bar{P}^{DA}[k+1] - \bar{P}^{DA}[k]\right) - \left(\hat{P}^{DA}[k+1] - \hat{P}^{DA}[k]\right)\right]^2 = \\ &= \frac{1}{T_h^2}\left[\frac{1}{n}\sum_{k=0}^{n-1}\left(\bar{P}^{DA}[k+1] - \hat{P}^{DA}[k+1]\right)^2 + \frac{1}{n}\sum_{k=0}^{n-1}\left(\bar{P}^{DA}[k] - \hat{P}^{DA}[k]\right)^2 - \frac{2}{n}\sum_{k=0}^{n-1}\left(\bar{P}^{DA}[k+1] - \hat{P}^{DA}[k+1]\right)\left(\bar{P}^{DA}[k] - \hat{P}^{DA}[k]\right)\right]\end{aligned} \tag{69}$$

Thus, using the definitions of load and VER forecast errors (9) and (10) respectively, the definition of the forecast error autocorrelation (11) and the definition of the VER penetration level (1), (68) can be written as:

$$\Delta R_{\varepsilon}^{DA}(t) = \left(\varepsilon_L^{DA} \cdot \frac{\sqrt{2\left(1 - \left(\rho_L^{DA}\right)^2\right)}}{T_h} \cdot \zeta_L^{DA}(t) - \varepsilon_V^{DA} \cdot \frac{\sqrt{2\left(1 - \left(\rho_V^{DA}\right)^2\right)}}{T_h} \cdot \pi \cdot \zeta_V^{DA}(t)\right) \cdot P_L^{peak} \tag{70}$$

where $\zeta_L^{DA}(t)$ and $\zeta_V^{DA}(t)$ are load and VER day–ahead ramping forecast error time series respectively, normalized to unit standard deviations. Thus, substituting (67) and (70) into (66), the mismatch term (22) takes the following form:

$$\begin{aligned}\Delta R^{DA}(t) = \left(\alpha_L \cdot \left(\bar{r}_L^{ST}(\alpha_L t) - \bar{r}_L^{DA}(\alpha_L t)\right) - \alpha_V \cdot \gamma \cdot \pi \cdot \left(\bar{r}_V^{ST}(\alpha_V t) - \bar{r}_V^{DA}(\alpha_V t)\right) + \right. \\ \left. + \varepsilon_L^{DA} \cdot \frac{\sqrt{2\left(1 - \left(\rho_L^{DA}\right)^2\right)}}{T_h} \cdot \zeta_L^{DA}(t) - \varepsilon_V^{DA} \cdot \frac{\sqrt{2\left(1 - \left(\rho_V^{DA}\right)^2\right)}}{T_h} \cdot \pi \cdot \zeta_V^{DA}(t)\right) \cdot P_L^{peak}\end{aligned} \tag{71}$$

$\Delta P^{ST}(t)$ mismatch term

The best short–term forecast profile (16) is used to split the mismatch term (23) into two components:

$$\Delta P^{ST}(t) = P(t) - \hat{P}^{ST}(t) = \left(P(t) - \bar{P}^{ST}(t)\right) + \left(\bar{P}^{ST}(t) - \hat{P}^{ST}(t)\right) = \Delta P_{\alpha}^{ST}(t) + \Delta P_{\varepsilon}^{ST}(t) \tag{72}$$

Each components is studied separately. Using (33) and (34), $\Delta P_{\alpha}^{ST}(t)$ can be written as:

$$\begin{aligned}\Delta P_{\alpha}^{ST}(t) &= P(t) - \bar{P}^{ST}(t) = \left(P_L(t) - \bar{P}_L^{ST}(t)\right) - \left(P_V(t) - \bar{P}_V^{ST}(t)\right) = \\ &= \left(\left(p_L(\alpha_L t) - \bar{p}_L^{ST}(\alpha_L t)\right) - \gamma \cdot \pi \cdot \left(p_V(\alpha_V t) - \bar{p}_V^{ST}(\alpha_V t)\right)\right) \cdot P_L^{peak}\end{aligned} \tag{73}$$

Next, $\Delta P_{\varepsilon}^{ST}(t)$ is represented as follows:

$$\begin{aligned}\Delta P_{\varepsilon}^{ST}(t) &= \bar{P}^{ST}(t) - \hat{P}^{ST}(t) = \left(\bar{P}_L^{ST}(t) - \hat{P}_L^{ST}(t)\right) - \left(\bar{P}_V^{ST}(t) - \hat{P}_V^{ST}(t)\right) = \\ &= \left(\frac{\bar{P}_L^{ST}(t) - \hat{P}_L^{ST}(t)}{\mathrm{std}\left(\bar{P}_L^{ST}(t) - \hat{P}_L^{ST}(t)\right)} \cdot \frac{\mathrm{std}\left(\bar{P}_L^{ST}(t) - \hat{P}_L^{ST}(t)\right)}{P_L^{peak}} - \frac{\bar{P}_V^{ST}(t) - \hat{P}_V^{ST}(t)}{\mathrm{std}\left(\bar{P}_V^{ST}(t) - \hat{P}_V^{ST}(t)\right)} \cdot \frac{\mathrm{std}\left(\bar{P}_V^{ST}(t) - \hat{P}_V^{ST}(t)\right)}{P_V^{max}} \cdot \frac{P_V^{max}}{P_L^{peak}}\right) \cdot P_L^{peak}\end{aligned} \tag{74}$$

Equation (74) contains identical expressions in form of standard deviations for load and VER profiles. Thus, it is calculated only once and the subscripts L,V are omitted [14]:

$$\begin{aligned}&\left[\mathrm{std}\left(\bar{P}^{ST}(t) - \hat{P}^{ST}(t)\right)\right]^2 = \frac{1}{T}\int_0^T \left(\bar{P}^{ST}(t) - \hat{P}^{ST}(t)\right)^2 \mathrm{dt} = \frac{1}{nT_m}\int_0^{nT_m} \left(\bar{P}^{ST}(t) - \hat{P}^{ST}(t)\right)^2 \mathrm{dt} = \frac{1}{n}\sum_{k=0}^{n-1}\frac{1}{T_m}\int_{kT_m}^{(k+1)T_m} \left(\bar{P}^{ST}(t) - \hat{P}^{ST}(t)\right)^2 \mathrm{dt} = \\ &= \frac{1}{n}\sum_{k=0}^{n-1}\frac{1}{T_m}\int_{kT_m}^{(k+1)T_m} \left[\left(\bar{P}^{ST}[k] - \hat{P}^{ST}[k]\right) + \frac{\left(\bar{P}^{ST}[k+1] - \hat{P}^{ST}[k+1]\right) - \left(\bar{P}^{ST}[k] - \hat{P}^{ST}[k]\right)}{T_m} \cdot t\right]^2 \mathrm{dt} = \\ &= \frac{1}{n}\sum_{k=0}^{n-1}\frac{1}{T_m}\int_{kT_m}^{(k+1)T_m} \left[\frac{\left(\left(\bar{P}^{ST}[k+1] - \hat{P}^{ST}[k+1]\right) - \left(\bar{P}^{ST}[k] - \hat{P}^{ST}[k]\right)\right)^2}{T_m^2} \cdot t^2 + \right. \\ &\left. + \left(\bar{P}^{ST}[k] - \hat{P}^{ST}[k]\right)^2 + 2 \cdot \left(\bar{P}^{ST}[k] - \hat{P}^{ST}[k]\right) \cdot \frac{\left(\bar{P}^{ST}[k+1] - \hat{P}^{ST}[k+1]\right) - \left(\bar{P}^{ST}[k] - \hat{P}^{ST}[k]\right)}{T_m} \cdot t\right] \mathrm{dt} = \\ &= \frac{1}{n}\sum_{k=0}^{n-1} \frac{\left(\bar{P}^{ST}[k+1] - \hat{P}^{ST}[k+1]\right)^2 + \left(\bar{P}^{ST}[k] - \hat{P}^{ST}[k]\right)^2 + \left(\bar{P}^{ST}[k+1] - \hat{P}^{ST}[k+1]\right)\left(\bar{P}^{ST}[k] - \hat{P}^{ST}[k]\right)}{3}\end{aligned} \tag{75}$$

Thus, using the definitions of load and VER forecast errors (9) and (10) respectively, the definition of the forecast error autocorrelation (11) and the definition of the VER penetration level (1), (74) can be written as:

$$\Delta P_{\varepsilon}^{ST}(t) = \left(\varepsilon_L^{ST} \cdot \sqrt{\frac{2 + \left(\rho_L^{ST}\right)^2}{3}} \cdot \xi_L^{ST}(t) - \varepsilon_V^{ST} \cdot \sqrt{\frac{2 + \left(\rho_V^{ST}\right)^2}{3}} \cdot \pi \cdot \xi_V^{ST}(t)\right) \cdot P_L^{peak} \tag{76}$$

where $\xi_L^{ST}(t)$ and $\xi_V^{ST}(t)$ are load and VER short–term forecast error time series respectively, normalized to unit standard deviations. Thus, substituting (73) and (76) into (72), the mismatch term (23) takes the following form:

$$\begin{aligned}\Delta P^{ST}(t) = &\left(\left(p_L(\alpha_L t) - \bar{p}_L^{ST}(\alpha_L t)\right) - \gamma \cdot \pi \cdot \left(p_V(\alpha_V t) - \bar{p}_V^{ST}(\alpha_V t)\right) + \right. \\ &\left. + \varepsilon_L^{ST} \cdot \sqrt{\frac{2 + \left(\rho_L^{ST}\right)^2}{3}} \cdot \xi_L^{ST}(t) - \varepsilon_V^{ST} \cdot \sqrt{\frac{2 + \left(\rho_V^{ST}\right)^2}{3}} \cdot \pi \cdot \xi_V^{ST}(t)\right) \cdot P_L^{peak}\end{aligned} \tag{77}$$

REFERENCES

[1] H. Holttinen, M. Milligan, B. Kirby, T. Acker, V. Neimane, and T. Molinski, "Using Standard Deviation as a Measure of Increased Operational Reserve Requirement for Wind Power," *Wind Engineering*, vol. 32, no. 4, pp. 355–377, 2008.

[2] P. J. Luickx, E. D. Delarue, and W. D. D'haeseleer, "Effect of the generation mix on wind power introduction," *Renewable Power Generation, IET*, vol. 3, no. 3, pp. 267–278, 2009.

[3] C. W. Hansen and A. D. Papalexopoulos, "Operational Impact and Cost Analysis of Increasing Wind Generation in the Island of Crete," *Systems Journal, IEEE*, vol. 6, no. 2, pp. 287–295, 2012.

[4] K. Bruninx and E. Delarue, "A Statistical Description of the Error on Wind Power Forecasts for Probabilistic Reserve Sizing," *Sustainable Energy, IEEE Transactions on*, vol. 5, no. 3, pp. 995–1002, 2014.

[5] B. C. Ummels, M. Gibescu, E. Pelgrum, W. L. Kling, and A. J. Brand, "Impacts of Wind Power on Thermal Generation Unit Commitment and Dispatch," *Energy Conversion, IEEE Transactions on*, vol. 22, no. 1, pp. 44–51, 2007.

[6] Y. V. Makarov, P. V. Etingov, and J. Ma, "Incorporating Uncertainty of Wind Power Generation Forecast Into Power System Operation , Dispatch , and Unit Commitment Procedures," *Sustainable Energy, IEEE Transactions on*, vol. 2, no. 4, pp. 433–442, 2011.

[7] Y. V. Makarov, S. Lu, N. Samaan, Z. Huang, K. Subbarao, P. V. Etingov, J. Ma, R. P. Hafen, R. Diao, and N. Lu, "Integration of Uncertainty Information into Power System Operations," in *Power and Energy Society General Meeting, 2011 IEEE*, 2011, pp. 1–13.

[8] Y. V. Makarov, C. Loutan, J. Ma, and P. de Mello, "Operational Impacts of Wind Generation on California Power Systems," *Power Systems, IEEE Transactions on*, vol. 24, no. 2, pp. 1039–1050, 2009.

[9] North American Electric Reliability Corporation, "Standard BAL-001-0.1a – Real Power Balancing Control Performance," NERC, Tech. Rep., 2012.

[10] A. Robitaille, I. Kamwa, A. Oussedik, M. de Montigny, N. Menemenlis, M. Huneault, A. Forcione, R. Mailhot, J. Bourret, and L. Bernier, "Preliminary Impacts of Wind Power Integration in the Hydro-Quebec System," *Wind Engineering*, vol. 36, no. 1, pp. 35–52, feb 2012.

[11] T. Aigner, S. Jaehnert, G. L. Doorman, and T. Gjengedal, "The Effect of Large-Scale Wind Power on System Balancing in Northern Europe," *Sustainable Energy, IEEE Transactions on*, vol. 3, no. 4, pp. 751–759, 2012.

[12] A. Muzhikyan, A. M. Farid, and K. Youcef-Toumi, "An Enhanced Method for the Determination of Load Following Reserves," in *American Control Conference 2014 (ACC2014)*, Portland, OR, 2014, pp. 926–933.

[13] A. Muzhikyan, A. M. Farid, and K. Youcef-Toumi, "An Enhanced Method for the Determination of the Ramping Reserves," in *American Control Conference 2015 (ACC2015)*, Chicago, Ill., 2015, pp. 994 – 1001.

[14] A. Muzhikyan, A. M. Farid, and K. Youcef-Toumi, "An Enhanced Method for the Determination of the Regulation Reserves," in *American Control Conference 2015 (ACC2015)*, Chicago, Ill., 2015, pp. 1016 – 1022.

[15] A. M. Farid and A. Muzhikyan, "The Need for Holistic Assessment Methods for the Future Electricity Grid," in *GCC CIGRE Power 2013*, Abu Dhabi, UAE, 2013, pp. 1–13.

[16] A. M. Farid, B. Jiang, A. Muzhikyan, and K. Youcef-Toumi, "The need for holistic enterprise control assessment methods for the future electricity grid," *Renewable and Sustainable Energy Reviews*, vol. 56, pp. 669–685, 2016. [Online]. Available: http://www.sciencedirect.com/science/article/pii/S1364032115012599

[17] B.-M. Hodge, D. Lew, M. Milligan, H. Holttinen, S. Sillanpää, E. Gómez-Lázaro, R. Scharff, L. Söder, X. G. Larsén, G. Giebel, D. Flynn, and J. Dobschinski, "Wind Power Forecasting Error Distributions: An International Comparison," National Renewable Energy Laboratory, Tech. Rep., 2012.

[18] B. Hodge and M. Milligan, "Wind Power Forecasting Error Distributions over Multiple Timescales," in *Power and Energy Society General Meeting, 2011 IEEE*. National Renewable Energy Laboratory, 2011, pp. 1–8.

[19] G. Giebel, R. Brownsword, G. Kariniotakis, M. Denhard, and C. Draxl, "The State-Of-The-Art in Short-Term Prediction of Wind Power: A Literature Overview," ANEMOS.plus, Tech. Rep., 2011.

[20] Federal Energy Regulatory Commission, "Order No. 764," FERC, Tech. Rep., 2012.

[21] N. Menemenlis, M. Huneault, and A. Robitaille, "Computation of Dynamic Operating Balancing Reserve for Wind Power Integration for the Time-Horizon 1–48 Hours," *IEEE Trans. Sustain. Energy*, vol. 3, no. 4, pp. 692–702, 2012.

[22] J. Kiviluoma, P. Meibom, A. Tuohy, N. Troy, M. Milligan, B. Lange, M. Gibescu, and M. O'Malley, "Short-term energy balancing with increasing levels of wind energy," in *Power and Energy Society General Meeting (PES), 2013 IEEE*, 2013, p. 1.

[23] K. De Vos and J. Driesen, "Dynamic operating reserve strategies for wind power integration," *Renewable Power Generation, IET*, vol. 8, no. 6, pp. 598–610, 2014.

[24] J. D. Lyon, F. Wang, K. W. Hedman, and M. Zhang, "Market Implications and Pricing of Dynamic Reserve Policies for Systems With Renewables," *Power Systems, IEEE Transactions on*, vol. 30, no. 3, pp. 1593–1602, 2015.

[25] F. Wang and K. W. Hedman, "Dynamic Reserve Zones for Day-Ahead Unit Commitment With Renewable Resources," *Power Systems, IEEE Transactions on*, vol. 30, no. 2, pp. 612–620, 2015.

[26] E. Ela, B. Kirby, E. Lannoye, M. Milligan, D. Flynn, B. Zavadil, and M. O'Malley, "Evolution of operating reserve determination in wind power integration studies," in *Power and Energy Society General Meeting, 2010 IEEE*, 2010, pp. 1–8.

[27] H. Holttinen, M. Milligan, E. Ela, N. Menemenlis, J. Dobschinski, B. Rawn, R. J. Bessa, D. Flynn, E. Gomez-Lazaro, and N. K. Detlefsen, "Methodologies to Determine Operating Reserves Due to Increased Wind Power," *Sustainable Energy, IEEE Transactions on*, vol. 3, no. 4, pp. 713–723, 2012.

[28] C. Wang, Z. Lu, and Y. Qiao, "A Consideration of the Wind Power Benefits in Day-Ahead Scheduling of Wind-Coal Intensive Power Systems," *Power Systems, IEEE Transactions on*, vol. 28, no. 99, p. 1, 2012.

[29] C. Monteiro, R. Bessa, V. Miranda, A. Botterud, J. Wang, and G. Conzelmann, "Wind Power Forecasting: State-of-the-Art 2009," Argonne National Laboratory, Illinois, Tech. Rep., 2009.

[30] E. Hirst, "Integrating Wind Energy With the BPA Power System: Preliminary Study," Tech. Rep., 2002.

[31] A. Muzhikyan, A. M. Farid, and K. Youcef-Toumi, "An Enterprise Control Assessment Method for Variable Energy Resource Induced Power System Imbalances. Part I: Methodology," *Industrial Electronics, IEEE Transactions on*, vol. 62, no. 4, pp. 2448–2458, 2015.

[32] A. Muzhikyan, A. M. Farid, and K. Youcef-Toumi, "An Enterprise Control Assessment Method for Variable Energy Resource Induced Power System Imbalances. Part II: Parametric Sensitivity Analysis," *Industrial Electronics, IEEE Transactions on*, vol. 62, no. 4, pp. 2459–2467, 2015.

[33] S. Frank and S. Rebennack, "A Primer on Optimal Power Flow: Theory, Formulation, and Practical Examples," Colorado School of Mines, Tech. Rep. October, 2012.

[34] E. Ela, M. Milligan, and B. Kirby, "Operating Reserves and Variable Generation," National Renewable Energy Laboratory, Tech. Rep., 2011.

[35] ENTSO-E, "Continental Europe Operation Handbook: P1. Load-Frequency Control and Performance," European Network of Transmission System Operators for Electricity (ENTSO-E), Tech. Rep., 2009.

[36] A. Muzhikyan, A. M. Farid, and K. Youcef-Toumi, "Relative merits of load following reserves & energy storage market integration towards power system imbalances," *International Journal of Electrical Power & Energy Systems*, vol. 74, pp. 222–229, 2016.

[37] A. Muzhikyan, A. M. Farid, and K. Youcef-Toumi, "A Power Grid Enterprise Control Method for Energy Storage System Integration," in *2014 IEEE PES Innovative Smart Grid Technologies Conference Europe (ISGT-Europe)*, Istanbul, Turkey, 2014, pp. 1–6.

[38] B. Jiang, A. Muzhikyan, A. M. Farid, and K. Youcef-Toumi, "Impacts of Industrial Baseline Errors in Demand Side Management Enabled Enterprise Control," in *41st Annual Conference of the IEEE Industrial Electronics Society (IECON2015)*, Yokohama, Japan, 2015, pp. 1–6.

[39] PJM, "Manual 12: Balancing Operations," PJM Interconnection, Tech. Rep., 2015.

[40] NERC, "Standard BAL-001-2 – Real Power Balancing Control Performance," North American Electric Reliability Corporation (NERC), Tech. Rep., 2013.
[41] J. Apt, "The spectrum of power from wind turbines," *Journal of Power Sources*, vol. 169, no. 2, pp. 369–374, jun 2007.
[42] A. E. Curtright and J. Apt, "The character of power output from utility-scale photovoltaic systems," *Progress in Photovoltaics: Research and Applications*, vol. 16, no. 3, pp. 241–247, may 2008.
[43] Bonneville Power Administration, "Wind Generation & Total Load in The BPA Balancing Authority." [Online]. Available: http://transmission.bpa.gov/business/operations/wind/
[44] P. Wong, P. Albrecht, R. Allan, R. Billinton, Q. Chen, C. Fong, S. Haddad, W. Li, R. Mukerji, D. Patton, A. Schneider, M. Shahidehpour, and C. Singh, "The IEEE Reliability Test System-1996. A report prepared by the Reliability Test System Task Force of the Application of Probability Methods Subcommittee," *Power Systems, IEEE Transactions on*, vol. 14, no. 3, pp. 1010–1020, 1999.
[45] E. A. DeMeo, W. Grant, M. R. Milligan, and M. J. Schuerger, "Wind plant integration: Costs, Status, and Issues," *Power and Energy Magazine, IEEE*, vol. 3, no. 6, pp. 38–46, 2005.
[46] J. C. Smith, M. R. Milligan, E. A. DeMeo, and B. Parsons, "Utility Wind Integration and Operating Impact State of the Art," *Power Systems, IEEE Transactions on*, vol. 22, no. 3, pp. 900–908, 2007.
[47] O. Edenhofer, L. Hirth, B. Knopf, M. Pahle, S. Schlömer, E. Schmid, and F. Ueckerdt, "On the economics of renewable energy sources," *Energy Economics*, vol. 40, Supple, no. 0, pp. S12–S23, dec 2013.
[48] C. Yuen, A. Oudalov, and A. Timbus, "The Provision of Frequency Control Reserves From Multiple Microgrids," *Industrial Electronics, IEEE Transactions on*, vol. 58, no. 1, pp. 173–183, 2011.
[49] Z. Zhou and A. Botterud, "Dynamic Scheduling of Operating Reserves in Co-Optimized Electricity Markets With Wind Power," *Power Systems, IEEE Transactions on*, vol. 29, no. 1, pp. 160–171, 2014.
[50] A. Ahmadi-Khatir, A. J. Conejo, and R. Cherkaoui, "Multi-Area Unit Scheduling and Reserve Allocation Under Wind Power Uncertainty," *Power Systems, IEEE Transactions on*, vol. 29, no. 4, pp. 1701–1710, 2014.
[51] M. H. Albadi and E. F. El-Saadany, "Comparative study on impacts of wind profiles on thermal units scheduling costs," *Renewable Power Generation, IET*, vol. 5, no. 1, pp. 26–35, 2011.
[52] IEA Wind, "Expert Group Report on Recommended Practices: 16. Wind Integration Studies," Tech. Rep., 2013.